Cell viability on functionalized diamond surfaces: towards non-invasive monitoring of cell characteristics

Nick SMISDOM

promotor :
dr. Martinus VAN DE VEN

co-promotor :
Prof. dr. Jean-Michel RIGO

Eindverhandeling voorgedragen tot het bekomen van de graad Master in de biomedische wetenschappen afstudeerrichting bio-elektronica en nanotechnologie

Universiteit Maastricht

universiteit hasselt

Preface

What once started as a slightly nervous day in a great, new world, now ends with writing this report. And although it had its good and bad sides, I won't regret a minute of the past four years. I learned many things and made a lot of new friends. Therefore, I hope this report is not the end but the beginning of a new adventure. An adventure that helps me in becoming a critical and skilled scientist.

Because science is teamwork, I would like to thank some people:

First of all, I would like to thank my promotor, Dr. Martin vandeVen. When you were around, all problems disappeared. Even when time was limited, I could rely on you.

Also my co-promotor, Prof. Dr. Jean-Michel Rigo, deserves a word of appreciation. I would like to thank you for making time to read and comment my draft document, to listen to my presentations and for your valuable advice.

I would also like to express my thanks to Prof. Dr. Marcel Ameloot. Thank you for critically reading my draft versions, for listening to my presentations and for giving valuable suggestions. Furthermore, when Martin was in the US, I could always count on you. Thank you so much!

Next, I would like to thank the great group at the department of cell physiology at Hasselt University. Many thanks to Dr. Ilse Smets for the valuable advice you gave me. Also many thanks to Mr. Johannes Janssen, Mrs. Rosette Beenearts and Mr. Patrick Pirotte as well as Mr. Johan Soogen and Mr. Roland van Werde to help me with all my practical problems. Of coarse, also many thanks to all Ph.D. students at the department. Whenever I had a question or a problem, you were always prepared to help me.

There are still other people I would like to thank. Special thanks to Dr. Oliver A. Williams, Ir. Michael Daenen en Dr. Ken Haenen, for supplying me with diamond. Without you, this report would not have been possible. Also many thanks to Prof. Dr. Ivo Lambrichts and Mr. Marc Jans for giving me advice about and logistic assistance with fixation procedures. Also many thanks to Mr. Kris Vanstreels, Mr. Bart Ruttens and Dr. Jan D'Haen for assistence with and access to the scanning electron microscope. I would also like to thank Prof. Dr. Valcke of the department of Biology for the use of their equipment. Also a special word of thanks to Mr. Jan Duchateau, Mr. Frederik Horemans en Mrs. Veerle Vrindts for doing the hard and dangerous work of cleaning the diamond substrates. Also special thanks to Ir. Ludo Naelaerts (KHLim) for borrowing his microscope. I would also like to thank Prof. Dr. Patrick Wagner, Dra. Sylvia Wenmackers, Drs. Peter Cooreman, Ir. Ronald Thoelen, Ir. Pieter Christiaens, and Dra. Veronique Vermeeren.

Of course, also a special word of thanks to my fantastic colleagues: Mieke, Debby, Ann and Kim. Thank you for the nice moments we shared in our office.

Finally I would like to thank my family: Joke, Leen, my mother and grandmother and my close friends. Thanks for your continuous support and trust in me.

Table of contents

List of figures

List of tables

List of abbreviations

α_2-GlyR	α_2 glycine receptor
μCD	microcrystalline diamond
2D	two-dimensional
3D	three-dimensional
CHO	Chinese hamster ovary (cell)
DLC	diamond-like carbon
DMSO	dimethyl sulfoxide
ECM	extracellular matrix
FACS	fluorescence activated cell sorter
FET	field effect transistor
HT	hydrogen terminated
MTT	3-(4,5 dimethylthiazol-2-yl)-2,5 diphenyl tetrazolium bromide
NCD	nano-crystalline diamond
OT	oxygen terminated
PI	propidium iodide
SEM	scanning electron microscopy/microscope
TRIS	TRIS-(hydroxymethyl)aminomethane

Summary

In this report both qualitative and quantitative results on cell viability of Chinese hamster ovary (CHO) cells cultured on bare, well-characterized nano- and microcrystalline diamond surfaces, either hydrogen or oxygen terminated, are presented and discussed. CHO cells stably transfected with homomeric embryonic α_2 glycine receptors are chosen since they offer a simplified cellular model. A systematic investigation of the viability is justified since earlier published reports are limited to more elaborate coated, single-crystal diamond surfaces.

Qualitative information was derived from visual inspection of the CHO cells on the microwave plasma-enhanced chemical vapor deposited (MPE-CVD) thin diamond films - deposited on silicon - using both scanning electron microscopy and optical reflection microscopy. Compared with control glass substrates, no apparent difference existed either in cell morphology or in cell density on all substrates tested.

In order to quantify these observations, other methods were applied. These consisted of different biochemical assays: the MTT cell proliferation assay (testing for proliferation and metabolic activity), the Bradford assay (total protein content), the [^{3}H]-thymidine cell proliferation assay (proliferation) and flow cytometry (living/necrotic/apoptotic cells). Consistent with the results obtained from visual inspection, no significant differences were found using one-way ANOVA. Yet, after 7 days post seeding, the MTT result did indicate significant differences between the tested substrates. However, this is not yet reproduced.

Based on these results, it can reasonably be conclude that, at least for the CHO cells used, bare nano- and microcrystalline diamond surfaces poorly affect, if at all, the growth and the viability of cultured cells

As a result, the diamond surfaces which are easiest to grow and to modify, with the best characteristics and the best shelf life, can be applied as substrate to develop non-invasive interfaces between biological cells on the one hand, and microelectronics on the other.

1 Introduction

The human body is a complex, three-dimensional system composed of a number of dedicated tissues, which in their turn consist of an assembly of communicating and cooperating cells. The latter are enclosed in and interact with their extracellular matrix (ECM). Health issues of the human body can often be reduced to a dysfunction at this cellular level. Therefore, methods for *in vitro* characterization of cellular behavior and function can contribute considerably to our knowledge of various complex diseases. However, current *in vitro* techniques used to investigate this cellular functionality have two important limitations. Firstly, many of these techniques are invasive which inherently leads to extra discomfort and stress, a relative time-limited characterization period and a possible confounding of the acquired data. Secondly, the two-dimensional (2D) nature of *in vitro* experiments is an often considerably simplified model of the real, complex three-dimensional (3D) environment in the body. This second limitation also may alter possible bi-directional interactions between cells, between the cell and the ECM and may introduce biasing interactions between cells and its artificial substrate [1].

1.1 A non-invasive interface

A first step towards a much improved characterization method is the construction of a 2D or 3D *non-invasive* interface between electronic components and individual biological cells or an ensemble of them. Due to its non-invasiveness, many potential deleterious effects of the method itself are ruled out and long-term characterization of cellular behavior and function becomes feasible. An example of such a technique is the multi-position planar electrode patch clamp method [2]. As a practical example of applications, such a non-invasive interface can be used to monitor a 2D-network of neurons or to monitor differentiation of stem cells.

A non-invasive interface with direct cell coupling can also advantageously be applied in cell-based biosensors. Once established, this methodology leads to relative straightforward biosensors in which the reaction of biological cells is monitored to detect potential beneficial pharmacological compounds and/or to determine the concentration of medically relevant substances. In combination with already established techniques to address living cells to the gate area of FET arrays [3,4], these sensors will be complementary to present high through-put screening methods. Moreover, the non-invasiveness together with the electronic readout of these biosensors are the fundaments to even more advanced biosensors. Sensors in which

the response of living, biological cells towards various stimuli can be used to control other biological cells, for example, to create an artificial retina.

Currently, an established way of constructing a functional non-invasive interface is the placement of a biological cell on the gate area of a field-effect transistor (FET; *Fig.1*) [5]. This causes the FET-channel to be modulated by membrane conductance changes and subsequent changes in membrane potential. Consequently, these modulations can be detected electronically. As a result, variations in the mentioned cell parameters caused by applied stressors are translated into electronic signals, providing the possibility of an automated, continuous monitoring of the biological response towards the stressor.

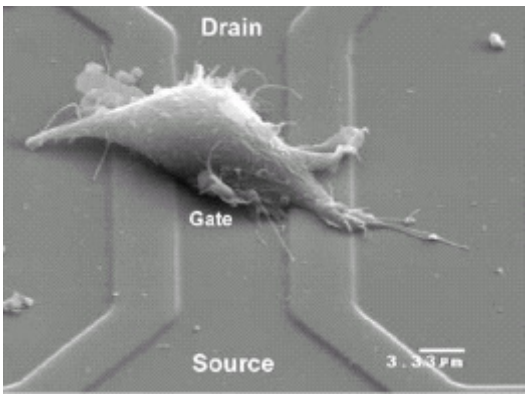

Fig.1: A biological cell on the gate area of a FET. On this scanning electron micrograph, a human embryonic kidney (HEK) 293 cell is located on the gate area of a FET. The surface layer consists of silicon dioxide coated with fibronectin. Scale bar is 3.33 µm. [6]

An often-applied material for such a non-invasive approach is silicon [5]. Due to its application in microelectronics, miniaturization techniques like lithography have been developed over the past 30 years to control shape and doping of this material at the sub-micron scale. This acquired knowledge, together with the scalability of this conventional semiconductor, was probably the main reason for its use as a substrate for a non-invasive interface. However, an ideal substrate should also fulfill other requirements, of which biocompatibility is the most important one. It has to be emphasized that biocompatibility has a rather broad scope and that a better description is necessary. Consequently, in this context, the term 'biocompatibility' refers to the absence of any confounding influence of the substrate on growth, behavior and function of the biological cell. Only many years after the first article about a possible non-invasive interface on silicon was published by Fromherz *et al.* [5], the biocompatibility of silicon, both bare and coated with several materials, was investigated and confirmed [7].

1.2 Diamond as a substrate for a non-invasive interface

Despite the previously mentioned qualities of silicon, diamond is a better substrate for a non-invasive approach. Besides its very well known mechanical hardness, it is chemically inert and can be used over a wide pH range. Consequently, in contrast to conventional semi-conductors, diamond will not corrode easily in cell growth media.

Secondly, diamond is optically transparent and has a large refractive index. This makes diamond very attractive for optical applications like total internal reflectance-based probing of interface regions, a method that monitors substrate interface interactions.

Thirdly, diamond surfaces, which are hydrogen terminated (HT) during the chemical vapor deposition (CVD), are hydrophobic and exhibit a p-type surface conductivity. Oxidized diamond surfaces are oxygen terminated (OT) and are hydrophilic. This difference offers an obvious procedure to surface patterning [8]. The HT surfaces, and not the OT surfaces, can easily be functionalized via various pathways to covalently attach biomolecules [9-12] or to create an anti-fouling surface [13].

Fourthly, the decreased thermal noise resulting from the wide band gap of diamond, can lead to a better signal-to-noise ratio as compared to conventional semi-conductors like silicon. Diamond can be doped with phosphorous or boron to create respectively n and p-type materials for p-n junctions and transistors. Very promising prototype-FETs with a functionalized gate surface area have already been produced using surface conductivity both on single crystal and polycrystalline diamond [14].

Finally, a very valuable property of diamond is its 'biocompatibility'. However, caution has to be taken when citing literature on this subject since most articles discuss about a totally different biocompatibility, i.e. the effect of diamond on the human body. In this sense, absence of monocyte stimulation by diamond particles [15], a relatively small amount of adsorbed fibrinogen on diamond [16,17], and a decreased adhesion and activation of polymorphonuclear leucocytes on diamond as compared to titanium [16] all indicate the inertness of diamond for the human body. Moreover, comparable results are also obtained with diamond-like carbon [18].

This bio-inertness in the human body offers the possibility of application in health and disease control devices. However, the use of diamond as a substrate for non-invasive interfaces between biological cells and electronic components requires, as stated above, the absence of any confounding influence of the substrate on growth, behavior and function of the biological cell. Published articles with respect to this subject are exceedingly sparse. In one article, the

growth of primary cortical neurons on laminin-patterned diamond is shown by Specht et al., but no quantitative investigation of cell viability was performed [19]. A second publication by Ariano et al., on the other hand, did investigate the influence of coated single-crystal diamond surfaces, both oxygen and hydrogen terminated, on neuronal cell growth and function, concluding that the surface termination of diamond has no significant influence [20]. As a consequence, diamond is considered to have no adverse effect on cellular parameters.

1.3 Chinese hamster ovary cells as a cellular model

Based on the aforementioned properties, diamond is an excellent substrate for a non-invasive interface between biological cells and electronic components. To facilitate the development of such an interface, Chinese hamster ovary (CHO) cells stably transfected with the embryonic homomeric α_2-glycine receptor (α_2-GlyR) [21] have been chosen as a cellular model. The use of this robust cell not only avoids the laborious work associated with primary cultures, it also reduces the variability within the cell population. Furthermore, it offers the opportunity to work with a very simple model in which only a few types of ion channels are expressed. This simplifies the interpretation of patch-clamp experiments and the cell characterization obtained by means of the non-invasive interface.

In addition to the advantages linked to this cell line, the ligand-gated nature of the ionotropic α_2-GlyRs brings about an extra advantage. In contrast to published articles with voltage-gated ion channels [22], the use of α_2-GlyRs allows electronic detection of a biological event, i.e. the binding of glycine to its receptor, via alterations in membrane conductance and membrane potential. On the short term, this can lead to the development of a biosensor for determination of the concentration of glycine or, when using an appropriate receptor, any ligand that results in a membrane potential change.

1.4 Research topic: quantifying a possible diamond-surface influence

CHO cells are cells with little or no preference of substrate. In other words, they grow on almost any surface. Consequently, the question that will be addressed in this work is whether CHO cells grow as well on bare diamond surfaces as on bare glass. As previously mentioned, research on this topic is very sparse and reports only deal with cell growth on single-crystal diamond coated with various adhesion molecules [19,20]. Furthermore, in this work more precisely nano- and microcrystalline diamond (*Fig.2*), either hydrogen or oxygen terminated, will be investigated and compared with control glass substrates. These results will be

complemented with flow cytometry results obtained with smooth H and O-terminated single-crystal type II diamond surfaces.

The different wettability accompanying the difference in termination of diamond surfaces, is known to affect cell adhesion and behavior. For CHO cells, hydrophilic plastic surfaces are known to promote cell adhesion, while hydrophobic surfaces impede cell adhesion [23]. Furthermore, topology is also an important factor. Zhu *et al.* clearly demonstrated the positive effect of parallel, nanoscale grooves on cell adhesion [23]. Although diamond surfaces are irregular, their topologies could influence cell adhesion and function. Moreover, differences between NCD and μCD can be expected. If these parameters of bare diamond surfaces indeed influence growth and function of CHO cells, a manner of specific cell positioning is retrieved. Hence, results presented in this report are of fundamental importance for the presented non-invasive methodology.

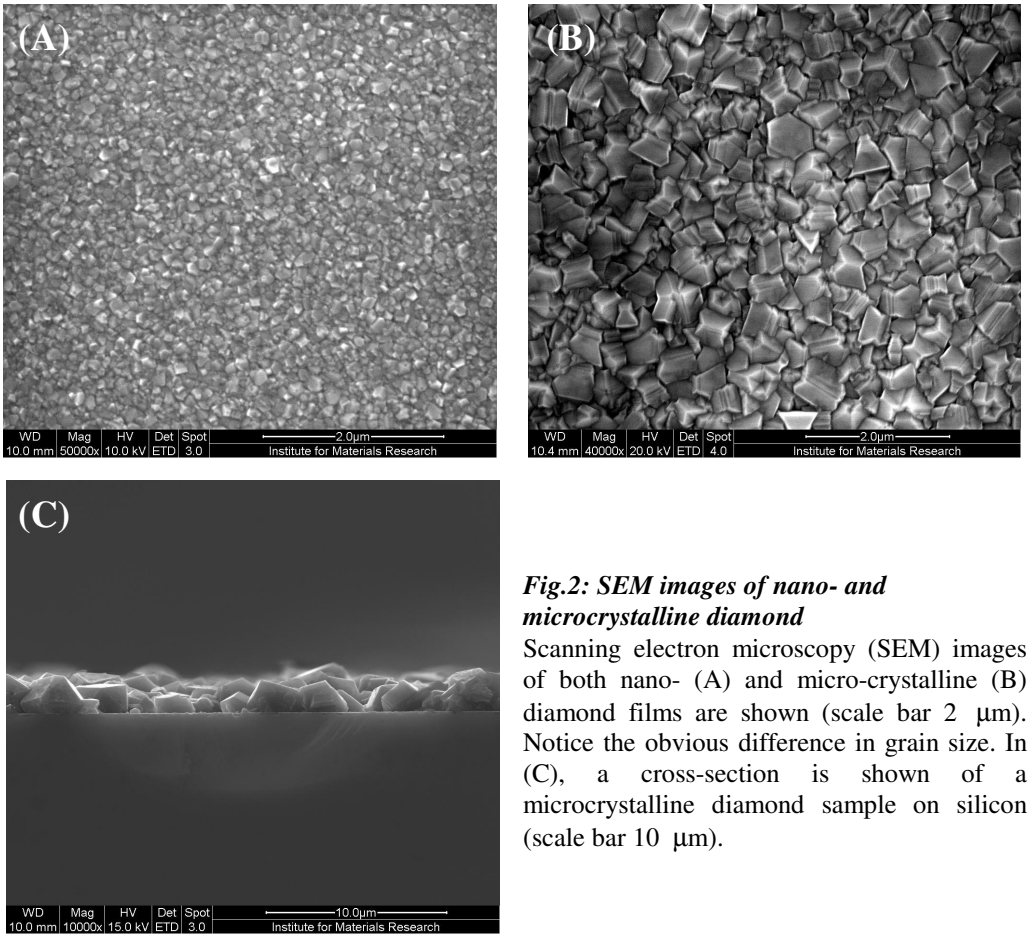

Fig.2: SEM images of nano- and microcrystalline diamond
Scanning electron microscopy (SEM) images of both nano- (A) and micro-crystalline (B) diamond films are shown (scale bar 2 μm). Notice the obvious difference in grain size. In (C), a cross-section is shown of a microcrystalline diamond sample on silicon (scale bar 10 μm).

1.5 Quantifying cell viability: the MTT cell proliferation assay

There are several methods to determine whether biological cells grow and keep their physiological functioning on a substrate. Of them, visual inspection of cell morphology and number is a necessary but subjective measure of cell viability. For this reason, several standard biochemical procedures have been used to better pinpoint cell growth and viability. Quantifying the number of dead and living cells can easily and reliably be achieved by flow cytometry. Cell proliferation, a general accepted measure for cell viability in the case of cell lines, can be assessed by measuring either proliferation itself or the resulting total cell number. Examples of these methods are respectively the [^{3}H]-thimidine cell proliferation assay and the Bradford assay for total protein content.

The colorimetric MTT cell proliferation assay, developed by T. Mosman in 1983 [24], is a procedure integrating both cell number and mitochondrial activity per cell [25]. Furthermore, this test is widely used to assess cytotoxicity of materials [25]. In a recent publication on cytotoxicity of DLC-coatings, however, it is stated that most of the MTT reduction occurs outside the mitochondrial inner membrane [26]. A closer examination of the literature on the MTT cell proliferation assay reveals some important facets of the test, which are described below. For a more detailed overview of this test, the interested reader is referred to a few selected articles [27-31].

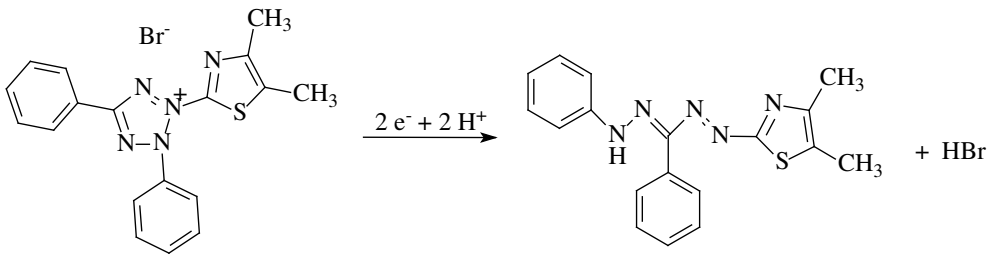

Fig.3: Reduction of MTT to formazan

Upon reduction of MTT to its formazan, the tetrazolium ring is opened and a molecule HBr is formed.

The MTT assay was originally developed and mainly used for high throughput screening to search for anticancer drugs [24,32]. Central to this assay is the reduction of water-soluble, yellow 3-(4,5 dimethylthiazol-2-yl)-2,5 diphenyl tetrazolium bromide (MTT) to water-insoluble, purple MTT-formazan (*Fig.3*) that can spectrophotometrically be detected [24]. Based on an article published in 1963 by Slater *et al.* [33], some more recent articles incorrectly state that this reduction was executed by the mitochondrial enzyme succinate dehydrogenase [34]. Conversely, Slater *et al.* clearly stated that there was no reactivity

between this enzyme and MTT [33]. Furthermore, based on cell homogenates and isolated mitochondria, two coupling points between MTT reduction and the mitochondrial respiratory chain, i.e. coenzyme Q en cytochrome c, are found [30,31,33]. Yet, MTT reduction in intact cells is not attenuated by mitochondrial respiratory chain inhibitors [30]. Moreover, increasing evidence does not support the exclusive role of mitochondria, but indicates an even more important role for NADH- and NADPH-dependent mechanisms in MTT reduction [29,30,35], which itself seems to enter the cell via endocytosis [30].

Besides the ill-understood reduction mechanism of MTT, attention should also be paid to the practical execution of the assay. Several pitfalls exist which have to be tightly controlled in order to obtain reliable results. A first important factor is the effect of MTT concentration and incubation time on the amount of MTT-formazan produced [34,35]. Because this factor is cell-type specific, the optimal MTT concentration and incubation time has to be determined for each cell type independently and therefore also for the CHO-cells. Secondly, the absorption of MTT-formazan is measured at various test and reference wavelengths without any regard for the actual applicability of published values (*Table 1*). This clearly indicates the need for determining the optimal test and reference wavelength. Thirdly, the absorbance spectrum of MTT-formazan changes and decreases with decreasing pH-value [27,36]. This constitutes a major, often overlooked systematic error. To rule out any pH effect, a buffer with a high pH value has to be used [27]. Fourthly, many solvents have been tried to dissolve the MTT-formazan crystals, but eventually dimethyl sulfoxide (DMSO) has been found to be the best solvent [36-38]. Finally, the reproducibility of the MTT assay is mainly influenced by the seeding of the cells. Therefore, a randomized design of the test procedure is of crucial importance [25].

When taking into account all these above factors, the MTT assay can indeed be used as a quantitative measure of a combination of cell proliferation and an integrated set of enzyme activities that are related in various ways to cell metabolism [28]. In addition, its rapidity, precision and lack of any radioisotope are important advantages of this test [24]. Most importantly, in combination with other tests like a Bradford assay to determine total protein content, the MTT assay can differentiate between an attenuated proliferation and an attenuated metabolism, which makes it a powerful tool.

Table 1: Overview of test and reference wavelengths used in published MTT assays

Test wavelength (nm)	Reference wavelength (nm)	Article
540	None	[35,38-41]
550	None	[37]
550	630	[42]
550	660	[26]
560	690	[34]
570	None	[27,29]
570	630	[24,30]
570	670	[25]
595	655	[43]

1.6 Research topic: practical execution

The question that was addressed in this work is whether CHO-cells grow as well on bare diamond surfaces as on bare glass. The work plan consisted of several phases. In a first phase, optical reflection microscopy and scanning electron microscopy was used to describe cell number and morphology. In a second phase, the MTT cell proliferation assay was optimized and applied to quantify any possible difference between the mentioned surfaces.

These results were complemented and compared with a) a Bradford assay to determine total protein content, b) a [^{3}H]-thymidine assay to measure cell proliferation, and c) flow cytometry using a calcein-AM / propidium iodide double staining to quantify fractions of living and dead cells.

Based on the obtained results, this report describes for the first time, as far as we are aware of it, both qualitative and quantitative results on cell viability on bare OT and HT nano- and microcrystalline diamond.

2 Material and Methods

2.1 Reagents and solutions

For cleaning procedures, spectrophotometric grade isopropanol was purchased from Sigma-Aldrich (Steinheim, Germany). Sulphuric acid, hydrochloric acid and potassium nitrate were all obtained from VWR Prolabo (Leuven, Belgium). Norvanol was prepared from 83.5 % alcohol (VWR Prolabo, Leuven, Belgium), 2.5 % ether (ACROS Organics, Geel, Belgium) and 14 % milli-Q water.

Cell culturing chemicals: high-sugar Dulbecco's modified Eagle's medium (DMEM), penicillin/streptomycin (10,000 U/ml and 10,000 μg/ml), Versene (1:5000), trypsin-EDTA (0.05 %) and trypsin (0.25%) were all purchased from Gibco (Paisley, UK). Fetal calf serum (FCS) was supplied by Hyclone Europe S.A. (Erembodegem-Aalst, Belgium). D-dextrose was obtained from VEL (Leuven, Belgium) and Zeocin™ from Invitrogen (Carlsbad, CA, USA). Phosphate Buffered Saline (PBS) buffer consisted of 130 mM NaCl, 1.54 mM KH_2PO_4, and 5.62 mM $Na_2HPO_4 \cdot 2H_2O$ (all purchased from Merck, Darmstadt, Germany). This PBS was always equilibrated with NaOH to pH 7.2, unless stated otherwise.
For cell fixation procedures, saccharose, paraformaldehyde, glutaraldehyde, Na-cacodylate and osmium tetroxide were all purchased from Sigma (Bornem, Belgium).

For MTT cell proliferation experiments, DMSO (spectroscopic grade), TRIS-(hydroxymethyl)aminomethane and NaCl were all purchased from ACROS Organics (Geel, Belgium). MTT (M 5655) and glycine were supplied by Sigma (Bornem, Belgium) and MTT-formazan by Fluka (Buchs, Switzerland). 'MTT assay solvent' consisted of DMSO with 15 % (v/v) 0.1 M TRIS-(hydroxymethyl)aminomethane buffer (TRIS buffer, adjusted to pH 10 with NaOH). Sorensen's glycine buffer consisted of 0.1 M glycine plus 0.1 M NaCl equilibrated to pH 10.5 with NaOH [27]. MTT stock solution contained 5 mg/ml MTT in CHO ringer. After filter sterilization (0.22 μm), this solution was stored at 4 °C in the dark and used within one month after preparation. CHO Ringer consisted of 140 mM NaCl, 2.5 mM KCl, 10 mM HEPES, 10 mM Glucose, 2 mM $CaCl_2$, and 1 mM $MgCl_2$, equilibrated to pH 7.2. All spectra were recorded with a Shimadzu UV/VIS scanning spectrophotometer UV-1600 PC (Shimadzu Benelux, Deurne-Antwerp, Belgium) with 1 nm step size, 0.1 second integration time, and approximately at room temperature (~ 20–23 °C). Solutions were placed in 1-cm

path length disposable poly-methylmethacrylate (PMMA) semi-micro cuvettes (high model; Kartell, Milan, Italy).

For Bradford assays, bovine serum albumin (BSA) was supplied by Sigma (Bornem, Belgium), NaOH by Merck (Darmstadt, Germany), Serva Blue G dye by Serva (Heidelberg, Germany), and ethanol (95 %) and phosphoric acid by VWR Prolabo (Leuven, Belgium).

Flow cytometry probes calcein-AM and propidium iodide (PI) as well as Pluronic® F-127 were purchased from Molecular Probes (Eugene, OR, USA). The loading buffer consisted of 20 nM calcein-AM (stock solution: 500 µM), 1 µg/ml PI (stock solution: 2.5 mg/ml) and 0.02 % (w/v) Pluronic® F-127 dissolved in PBS.
For microfluorimetry, the loading buffer consisted of 1 µM calcein-AM and 1µg/ml PI dissolved in CHO ringer. Both loading buffers were used within 3 hours of preparation.

2.2 Diamond and glass substrates

Nano- and micro-crystalline diamond as well as single crystal diamond was kindly provided by the Institute of Materials Research (IMO, Diepenbeek, Belgium). Both nano- and micro-crystalline diamond were grown via microwave plasma-enhanced chemical vapor deposition (MPECVD) on silicon wafers of 5 cm diameter. It has to be mentioned that the nano-crystalline wafers were heterogeneous in color, while the microcrystalline ones were rather homogeneous. Coated wafers were cut with a diamond cutting pen into samples of about 1 cm^2. Half of the total number of these hydrogen terminated samples was made oxygen terminated by placing them for half an hour in a mixture of 1 % (w/v) potassium nitrate in sulphuric acid at 250 ºC. After each experiment, samples were regenerated by placing them for 2 hours in boiling hydrochloric acid under a fume hood.
Single crystals of different orientation were used, i.e. 111 and 100 (Sumitomo, Tokyo Japan), with square surface areas of respectively 6.25 and 4 mm^2. These were made either hydrogen terminated via half an hour in hydrogen plasma or oxygen terminated in a strong oxidative acidic mixture as described above.
The glass substrates used as control, consisted of five groups. Three of them were 12 mm round, 10 mm square and 10 mm round glass (coverslips, all Menzel Gläser, Braunschweig, Germany). The other two groups were pieces of cut microscope slides (Menzel Gläser, Braunschweig, Germany) to sizes of 2 x 2 mm and 2.5 x 2.5 mm.

2.3 Cell culture

CHO-cells stably transfected with the embryonic homomeric α_2-GlyR were provided by B. Rogister (CNCM, Ulg) [21]. They were cultured and maintained in high-sugar Dulbecco's modified Eagle's medium supplemented with 10 % heat-inactivated fetal calf serum, 13.9 mM D-dextrose, 5 µg/ml zeocin™, and 2 % penicillin/streptomycin and incubated in a humidified atmosphere of 5% CO_2 and 95 % air at 37 °C.

All diamond samples were kept at least 24 hour in isopropanol and were blown dry with wet nitrogen. Glass control substrates, kept at least 24 hour in norvanol, were rinsed briefly in isopropanol and air dried. To sterilize the substrates, they were kept for 2 hours at 180 °C.

After 1 minute incubation with Versene, CHO-cells were trypsinated with trypsin-EDTA for 3 minutes, after which the trypsin was inactivated with cell growth medium. The resulting cell suspension was centrifuged for 10 minutes at 1300 rpm with a Jouan B3.11 (Thermo electron corporation, Waltham, MA, USA) and the cell pellet was resuspended in fresh cell growth medium. After determining the cell density with a Fuchs-Rosenthal counting chamber, cells were seeded well-dispersed at a density of 7,500 cells cm^{-2} on the uncoated substrates in 24-well plates (Nunc™, Roskilde, Denmark). Cells were cultured under the same conditions as for normal cell culturing described above. Diamond and control glass substrates were incubated in the same 24-well plate in a randomized manner to equalize all parameters. For all experiments, 8 passages of the cells were not exceeded. All experiments were performed in the exponential growth phase between 5 and 7 days post seeding, after transferring the substrates to new 24-well plates.

2.4 Visual inspection by Scanning electron microscopy and optical reflection microscopy

Cell morphology and density was observed with a Quanta 200-FEG scanning electron microscope (SEM; FEI Corp., Hillsboro, OR., USA). CHO cells were cultured for 5 days. Cell growth medium was aspirated and replaced with 4% (v/v) paraformaldehyde dissolved in PBS pH 7.3. After 10 minutes incubation, this fixative was aspirated and replaced by PBS pH 7.2, preceding a new 10 minute incubation period. After repeating this last step, the fixated cells were prepared for SEM imaging by dehydration in an alcohol series (30, 50, 70, 90, and 100%). For cells on diamond substrates, SEM images were taken in high vacuum (~ 10^{-5} mbar) while cells on glass substrates were taken in low vacuum (~ 0.9 mbar) using water vapor to prevent charging of the substrates.

To improve the contrast, the following procedure was tried. After aspiration of the cell growth medium, the samples were rinsed three times for 5 minutes with cacodylate buffer (0.03 M Na-cacodylate, 12.8 g saccharose). Next, cells were fixated for 10 minutes with 2 % (v/v) glutaraldehyde in 0.03 M Na-cacodylate pH 7.3. Followed by again 2 wash steps of each 5 minutes with cacodylate buffer, cells were treated with osmium tetroxide for 10 minutes. After rinsing with distillated water, cells were dehydrated as described above.

Due to the non-transparent nature of the NCD and μCD silicon substrates, traditional transmission light-microscopy could not be used. Therefore, two other systems, based on optical reflection microscopy, were tried. The first setup (*Fig.4*) consisted of an upright stereo-microscope (SMZ-2T, Nikon, Japan) with a digital camera (4x optical zoom, Coolpix MDC lens; Coolpix 5400, Nikon, Japan) and fiber optics (intralux 150 H, Volpi, Zürich, Swiss). Contrast was optimized by repositioning the external fiber optic bundles. In a second method, the cells were illuminated along the same optical path as the observation takes place by using a dichroic mirror and/or in combination with excitation and emission polarizers (Nikon Optiphot, Nikon, Japan).

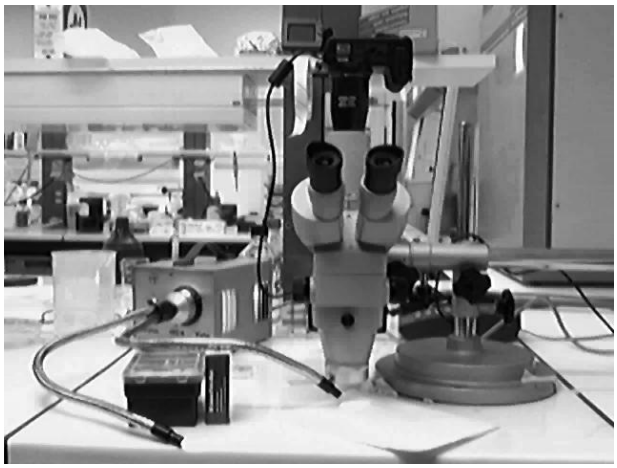

Fig.4: First setup used for optical reflection microscopy

This consisted of an upright stereo-microscope (SMZ-2T, Nikon, Japan) with a digital camera (4x optical zoom, Coolpix MDC lens; Coolpix 5400, Nikon, Japan) and fiber optics (intralux 150 H, Volpi, Zürich, Swiss).

2.5 MTT cell proliferation assay

Before applying the MTT cell proliferation assay on cells grown on diamond substrates, several factors had to be optimized. Besides the concentration and time-dependence of the assay, the optimal test and reference wavelengths were determined as well as the effects of a buffer with a high pH value. The MTT assay was tested to assess the influence of the cell seeding procedure and the reliability of the procedure used to normalize to 1 cm^2. Finally, the experiments with the diamond substrates were carried out.

2.5.1 Optimization

To determine the optimal test and reference wavelengths, MTT assay solvent was used to resemble the conditions found at the end of the MTT assay. Following concentrations were used: blank DMSO/TRIS buffer, 1 mg/ml MTT, 6 % (v/v) cell growth medium and 0.05 M MTT-formazan, all dissolved in the MTT assay solvent. Absorbance spectra were recorded from 370 nm to 800 nm with a Shimadzu UV-1600 PC scanning spectrophotometer. These measurements were complemented with a spectrum of cellular reduced MTT-formazan derived from a MTT assay executed on the diamond substrates.

For verification of the results published by Plumb *et al.* [27], the pH-dependence of MTT-formazan was investigated. Three solutions were made: DMSO acidified with 0.04 N HCl, neat DMSO and MTT assay solvent, all with a MTT-formazan concentration of 0.04 M. Absorbance spectra were obtained as described above.

Besides the pH dependence, the stability of MTT in the presence of a Sorensen's glycine buffer was also tested. Using the scanning spectrophotometer, absorbance of a 0.5 M MTT solution in DMSO was read at 550 nm during 5 minutes. Between the first 20 and 32 seconds, Sorensen's glycine buffer was added to a final concentration of 11.1 % (v/v) as described by Plumb *et al.* [27]. This was repeated with TRIS buffer pH 10 (final concentration: 15 % (v/v))

Because MTT was found to be more stabile in TRIS buffer, the optimal concentration of this buffer in DMSO was determined. Starting with 800 µl of a 0.04 M MTT-formazan solution in neat DMSO, following volumes of TRIS buffer pH 10 were added in a successive manner: 10 times 0.5 µl, 5 times 1 µl, 8 times 5 µl, and 6 times 25 µl. Of each solution, an absorbance spectrum was recorded as described above.

The interference of cell growth medium is a frequently mentioned problem in the literature about MTT assays. This interference is investigated by adding cell growth medium to various solutions in the same way as done for optimization of the TRIS buffer content. The used solutions were 0.04 M MTT-formazan in neat DMSO, 0.04 M MTT-formazan in MTT assay solvent and 0.04 M MTT-formazan in DMSO with 11.1 % (v/v) Sorensen's glycine buffer. Absorbance spectra were obtained as described above. These results were compared with published results of Plumb *et al.* [27].

The effect of the cell growth medium is expressed as the relative error. This is the difference in absorbance between presence and absence of the cell growth medium, divided by the absorbance in absence of cell growth medium and multiplied by 100. To better compare both TRIS and Sorensen's glycine buffer, their effect is expressed as the relative correction of the medium influence. This is calculated by first dividing the relative error in presence of the respective buffer by the relative error in absence of the buffer, followed by subtracting the resulting number from 100.

The residual volume of cell growth medium left after aspiration of the incubation medium was estimated. A 24-well plate was filled with 24 diamond substrates. After weighing (Sartorius model n° 1872, Goettingen, Germany), 600 µl milli-Q water (Millipore, Billerica, MA, USA) was added to each well and aspirated again as much as possible. The 24-well plate was weighted again. The resulting difference between the last and the first weighing was divided by 24, leaving the weight of the average residual water volume.

After optimization of the absorbance readings, cell specific parameters were optimized. The optimal MTT concentration was determined using freshly trypsinated cells (as described in *Cell culture*). 55 eppendorf® tubes (1.8 ml; Kartell, Milan, Italy) were filled with 600 µl cell suspension in cell growth medium with a density of 250,000 cells/ml. These cell suspensions were incubated for 1 hour at 37 °C with following final concentrations: 0, 0.1, 0.2, 0.3, 0.4, 0.5, 0.72, 1, 1.25, 1.54, and 2 mg/ml (every concentration in five fold). After centrifugation at 7500 rpm and 4 °C (Centrifuge 5804R, Eppendorf Ag, Hamburg, Germany), the supernatant containing the unreduced MTT was aspirated. Next, 800 µl MTT assay solvent was added to dissolve the MTT-formazan crystals and absorbance spectra were recorded within 2 minutes as described above.

The time-dependence of the MTT assay was investigated by using a 1 hour as well as a 4 hour incubation period. A serial dilution of cell densities (from 4,000,000 to 21,000 cells/ml) was

made, and 600 µl of each cell suspension was put in 1.8 ml-eppendorf® tubes in ten fold. To each tube, 150 µl MTT stock solution (5 mg/ml) was added. After respectively 1 and 4 hours, 5 tubes of each density were centrifuged as described above. Next, the incubation medium was aspirated and the MTT-formazan crystals were dissolved in MTT assay solvent in such a way that the measured absorbances were within the linear range of the spectrophotometer. Absorbance spectra were recorded within 2 minutes as described above.

Possible confounding influences of the seeding of the cells itself [25] or of the size and shape of the surface area of the substrates were investigated. Both experiments were executed as stated below (see *Application of the cell proliferation assay*). The substrates used for the first experiment were all square, glass substrates of 1 cm^2. As a consequence, any variation found in the assay was solely due to the cell seeding. The substrates of the second experiment contained 3 categories: 12 mm round, 10 mm square and 10 mm round glass substrates. Knowing the variation due to the seeding, the resulting variation in this experiment leads to information on the method used to correct for the difference in surface area.

2.5.2 Application of the cell proliferation assay

The general procedure of the MTT cell proliferation assay was as follows. After 5 to 7 days of exposure to the stressor, in this case the growth on the different substrates, MTT stock solution (5 mg/ml) was added to 20 % (v/v) of the final volume (final concentration was 1 mg/ml). To avoid any influence of the surrounding cell layer on the bottom of the well, the substrates were prior to this addition transferred to a new 24-well plate containing 600 µl fresh cell growth medium. After 1 hour incubation at 37 °C, the incubation medium was aspirated as much as possible and the plate was wrapped in tin foil. The MTT-formazan crystals were dissolved with MTT assay solvent and transferred to 1-cm path length disposable PMMA semi-micro cuvettes. Absorbance spectra were recorded from 370 nm to 800 nm and were all corrected for the MTT assay solvent. Subsequently, absorbance at 550 nm minus absorbance at 800 nm was used as the final absorbance value.

To investigate if the color difference of the nanocrystalline wafers has a significant influence, 4 blue and 4 yellow NCD samples were compared. In two other experiments, the difference between NCD and µCD, both HT and OT, was investigated.

2.6 Bradford assay

After 6 days post seeding, a Bradford assay was executed to determine the total protein content. The calibration curve for this assay was based on a serial dilution of bovine serum albumin from 1000 to 7.81 µg/ml dissolved in 0.1 N NaOH. The color reagent consisted of 0.1 g/ml Serva Blue G dye, 0.05 % (v/v) ethanol 95 %, and 0.1 % (v/v) phosphoric acid. Cell growth medium was aspirated and collected in separate 1.8 ml-eppendorf® tubes. Substrates were transferred to a new 24-well plate and rinsed once with PBS pH 7.2. This PBS buffer was collected in the same tubes as the aspirated cell growth medium and centrifuged for 10 minutes at 2000 rpm 37 °C (Centrifuge 5804R, Eppendorf Ag, Hamburg, Germany). After aspiration of the supernatant, the pellet was resuspended in 250 µl of 0.1 N NaOH. During centrifugation, 500 µl 0.1 N NaOH was added to each well as well as the 250 µl from the tubes. Following an incubation period of 15 minutes at 37 °C, 20 µl of each well was added to four replicate wells of a flat-bottom 96-well plate. This was also done for the serial dilution of the calibration curve and for blanco 0.1 N NaOH solution. After addition of 270 µl reagent to each well, the plate was incubated for 10 minutes and absorbances were measured at 630 nm with an ELISA plate reader (ICN Biomedicals, Asse, Belgium).

2.7 [^{3}H]-Thymidine cell proliferation test

The [^{3}H]-thymidine cell proliferation test was executed after 6 days post seeding. 16 hour prior to the experiment, substrates were transferred to a new 24-well plate and incubated with 1 µCi/ml tritium-thymidine [^{3}H]-thymidine; Amersham Biosciences, Diegem, België) [44,45]. Cell growth medium was aspirated and collected in 1.8 ml-eppendorf® tubes. The substrates were rinsed once with PBS pH 7.2, which was collected subsequently in the same tubes. After 10 minutes centrifugation at 3500 ×g (Biofuge 15; Heraeus Sepatech, Osterode, Germany), the supernatant was removed. Cells were trypsinated with 0.25 % trypsin / 1 mM EDTA (UCB, Brussels, Belgium) during 3 minutes. Trypsin was inactivated with 60 µl FCS and the cell suspension was transferred to the corresponding tubes. Substrates were rinsed with PBS pH 7.2, which again was collected. After a second centrifugation step, the resulting pellet was resuspended in 200 µl PBS pH 7.2 and transferred to a 96-well plate. Next, the cellular material was harvested on glass-fiber filter with a Filtermate harvester (PerkinElmer, Wellesley, MA, USA). The filters were dried and the incorporated radioactive material was measured in 5 ml scintillation fluid (Wallac, Turku, Finland) in a 1450 MicroBeta JET liquid scintillation counter (PerkinElmer, Wellesley, MA, USA).

2.8 Flow cytometry

Fractions of living and dead cells were determined by means of flow cytometry. To discriminate between these fractions, the combination calcein-AM and propidium iodide was used. Calcein-AM is a nonfluorescent calcein acetoxymethyl ester that can easily cross cellular plasma membranes. Once inside the cell, it is hydrolyzed to green-fluorescent, hydrophilic calcein by intracellular esterases present in living cells. Propidium iodide (PI), on the other hand, is positively charged and can not cross intact plasma membranes. However, necrotic cells don't have an intact plasma membrane anymore. This allows PI to enter the cell and to intercalate with DNA and RNA, enhancing its fluorescence significantly.

After 5 days post seeding, the cell growth medium was aspirated and collected in 1.8 ml-eppendorf® tubes. The supernatant was removed after 10 minutes centrifugation at 2000 rpm at 37 °C (Centrifuge 5804R, Eppendorf Ag, Hamburg, Germany). The cell pellet was resuspended in 150 µl PBS pH 7.2 and transferred to a 96-well plate with v-bottom. Meanwhile, the substrates were transferred to a new 24-well plate. Cells were trypsinated with 0.25 % trypsin / 1 mM EDTA during 3 minutes. After inactivation of trypsin with FCS, the cell suspension was transferred to the same 96-well plate. Substrates were rinsed with PBS pH 7.2, which again was transferred to the 96-well plate. After centrifugation of this plate for 10 minutes at 1500 rpm (Centrifuge 5810, Eppendorf Ag, Hamburg, Germany), supernatant was aspirated and cell pellet was resuspended with PBS pH 7.2. The centrifugation step was repeated and, after aspiration of the supernatant, the cell pellets were resuspended and incubated in the dark at room temperature with flow cytometry loading buffer. After 10 minutes, fractions of living, necrotic and apoptotic cells were determined using a FACS (FACScan; Becton Dickinson, San Jose, CA, USA).

Due to the small surface area of the single crystal substrates, these samples were only analyzed using microfluorimetry. In short, this method can be considered as an '*in situ*' method of the flow cytometry. Substrates with the cell monolayers were incubated with 1 µM calcein-AM and 1µg/ml PI, dissolved in CHO ringer. After 10 minutes incubation in the dark at about 20 °C, confocal fluorescence microscopy was carried out with a Zeiss LSM 510 META system (Zeiss, Jena, Germany). Settings were 10x, NA 0.3 and pixel dwell time of 25.6 µs. Images were recorded using a multitrack. Calcein fluorescence was measured with 1 % 488 nm excitation (Ar-ion laser) and 500-550 nm emission band pass filter. PI fluorescence

was measured with 10 % 543 nm excitation (green-Ne laser) and 565-615 nm emission band pass filter. Image size was 512 x 512 pixels.

2.9 Data analysis

All data were processed using Excel (Microsoft Corp, Portland, OR, USA). Graphing and statistical analysis was performed using Prism® 4 (GraphPad Software, Inc., San Diego, CA, USA). All data of the MTT cell proliferation assay, Bradford Assay and [^{3}H]-thymidine cell proliferation assay were normalized to 1 cm^2 surface area and all data were normalized to the values obtained with respective glass controls. Normalization to 1 cm^2 surface area was done as follows. First, the volume of cell suspension put on the substrates was dependent on this surface area. For example, if a substrate was only 0.85 cm^2, then only 85 % of the volume for 1 cm^2 was used. Secondly, the resulting absorbance value of the MTT assay was divided for each sample by its surface area (in cm^2). At the end, all obtained values were normalized to 1 cm^2.

Confocal microscopy images were processed with Java based ImageJ and its plugins (NIH, Research Services Branch, Bethesda, MB, USA). After sharpening, contrast enhancement and histogram stretching accompanied at times with radius 100 rolling ball background subtraction, a threshold was selected appropriate for discriminating between background and Calcein / PI related pixels. Converted to binary, all images were noise despeckled when necessary and the watershed segmentation was applied. Using particle counting statistics the total number of cells in each image was determined. Lower particle size limit was chosen to eliminate any small pixel clusters not related to cell areas. Oxygen terminated samples possessed a rather high background and were just thresholded before the watershed algorithm was applied.

All data were, when possible, analyzed using one-way ANOVA with a Bonferroni post test to compare with glass controls, and with two-way ANOVA to search for significant influence of either crystallinity or surface termination. All p-values lower than 0.05 % were considered significant. Error bars represent one standard error of the mean (S.E.M.). The number of samples n is either printed in the figure or mentioned in the legend.

3 Results

Several optical and biochemical methods have been used to characterize the cell-diamond surface interactions with glass surface as a control (*Table 2*).

Table 2: Schematic overview of techniques applied

Visual inspection	
Scanning electron microscopy	19
Optical reflection microscopy	22
Biochemical methods	
MTT cell proliferation assay	
Optimization	
Determination of the optimal test and reference wavelength	23
pH-dependence of MTT-formazan absorbance	24
Stability of MTT in DMSO in the presence of buffers	25
Optimal v/v % of TRIS buffer in DMSO	25
Interference of cell growth medium	25
Optimal final MTT concentration	27
Optimal incubation time	27
Influence of the seeding of the cells	28
Control method to normalize all substrates to 1 cm^2	28
Control for heterogeneous color of nanocrystalline wafers	29
Application of the MTT cell proliferation assay	30
Bradford assay to determine total protein content	31
[^{3}H]-thymidine cell proliferation assay	32
Flow cytometry to determine fractions of living, necrotic and apoptotic cells	32
Microfluorimetry on single crystal diamond substrates	34

3.1 Visual inspection using scanning electron microscopy and light reflection microscopy

In this first phase, visual inspection of cell morphology and density was carried out. An obvious monolayer could be seen at 5 days post seeding on SEM images of both nano- and microcrystalline diamond (*Fig.5*). On the microcrystalline diamond, the cell membrane sometimes followed the crystals deliniation, although this was not always the case.

Comparison of cell morphology with the one on glass was difficult, because SEM-images had to be taken in low vacuum and this resulted in poor contrast (*Fig.6*). However, post fixation with osmium tetroxide improved the contrast on glass and a monolayer comparable with the ones seen on diamond surfaces, could be seen. Conversely, postfixation of cells on diamond substrates with osmium tetroxide reduced the contrast. Apparently, regardless of their termination, there were no large differences in CHO cell growth between the substrates.

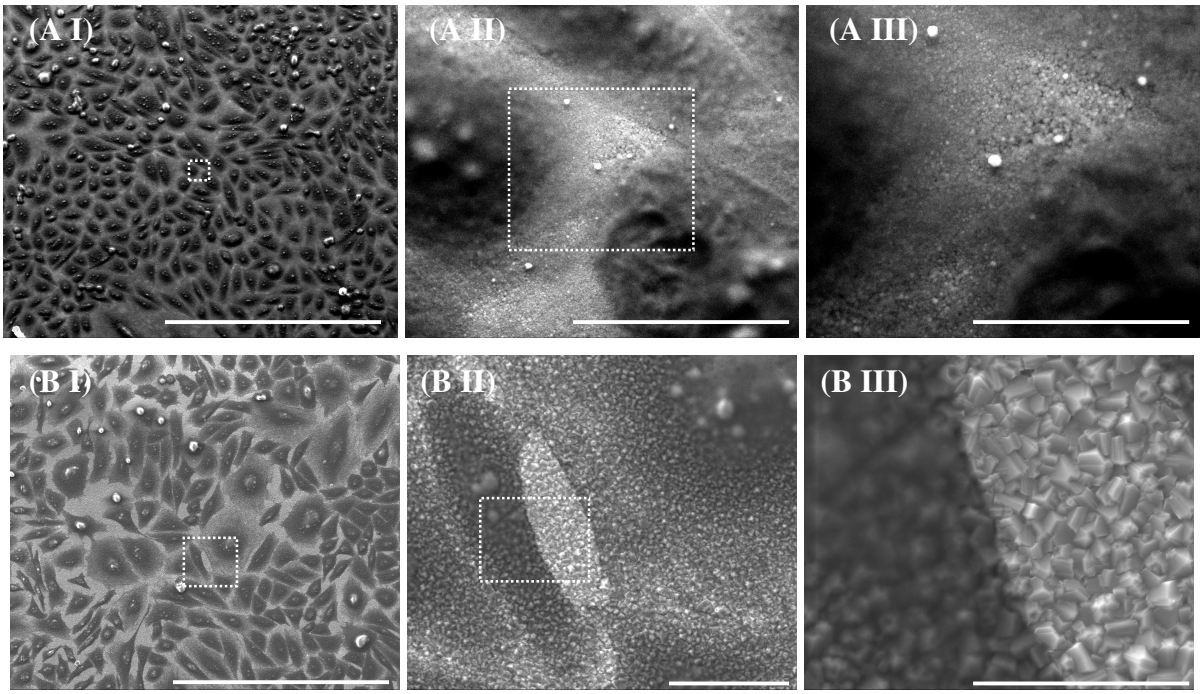

Fig.5: Scanning electron microscopy images of CHO cellular monolayers on diamond

After 5 days post seeding, cells grown on OT-NCD (A) and HT-μCD (B) were fixated and dehydrated. These images show a monolayer of apparently healthy cells on top of the diamond surfaces. Scale bars are 300 μm (A I, B I), 20 μm (A II, B II) and 10 μm (A III, B III). Dotted squares indicate the place of larger magnifications.

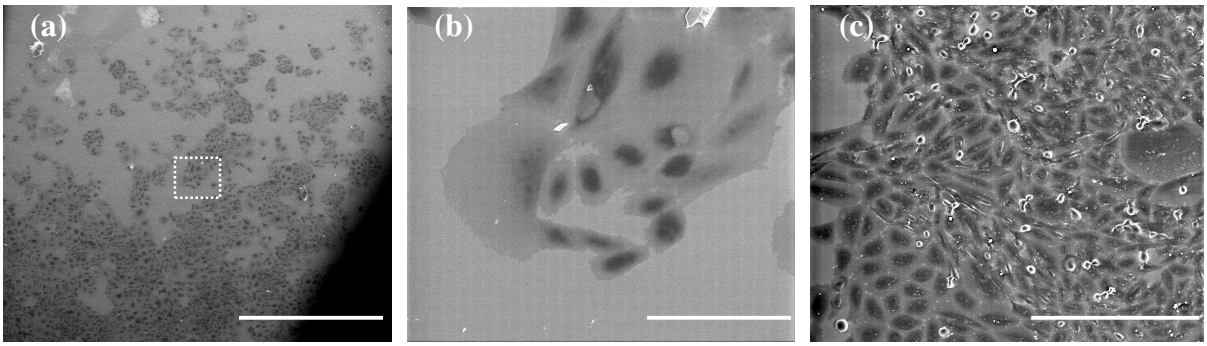

Fig.6: SEM images of CHO cells on glass substrates

After 5 days post seeding, cells grown on control glass substrates were fixated and dehydrated (a and b). At the bottom of (a), a sub confluent monolayer can be seen. (c) Same conditions, except a post fixation with osmium tetroxide between fixation and dehydration. The contrast is improved and a monolayer comparable with the ones on diamond surfaces can be seen. Scale bars are respectively 1 mm, 100 μm and 200 μm. Dotted square indicates the place of which (b) is a magnification.

Although osmium tetroxide diminishes contrast of diamond substrates it does have another advantage. It allowed for an excellent resolution of the cells when tilting the substrate 45 ° with respect to the incoming scanning e-beam. This generated a 3D view of the monolayer. In contrast to Zhu et al.[23], we observed that a confluent monolayer was present on the substrates, but some aggregates of cells were present on top of this layer (*Fig.8*).

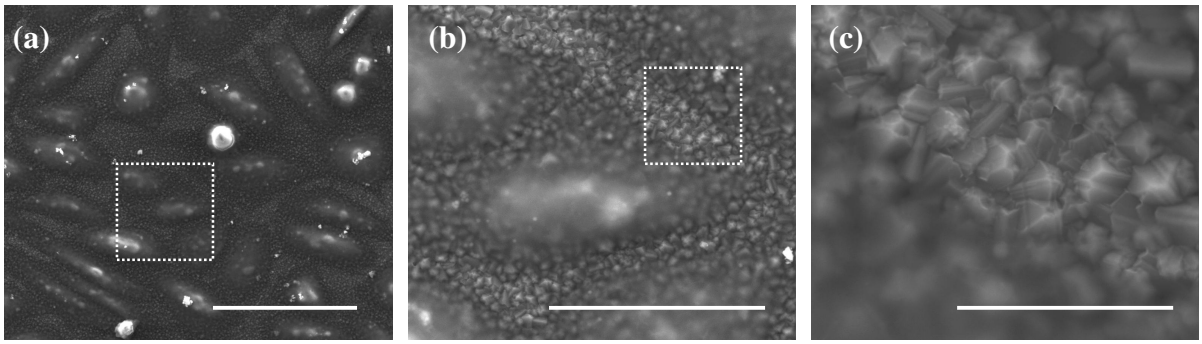

Fig.7: Post fixation with osmium tetroxide of cells on diamond substrates

After 5 days post seeding, CHO cells grown on OT-NCD were fixated, post fixated with osmium tetroxide and dehydrated. The contrast is decreased. Scale bars are respectively 50 µm, 20 µm and 5 µm. Dotted lines indicate places of larger magnifications.

Fig.8: A tilt-corrected SEM-image of a confluent monolayer of CHO cells on control glass surfaces

After 5 days post seeding, cells grown on glass were fixated, post fixated with osmium tetroxide and dehydrated. The glass substrate was tilted 45 ° with respect to the incoming e-beam. Besides the confluent monolayer of cells, some aggregates (arrow) can be seen. Scale bar is 400 µm.

Since the diamond-layer covered silicon substrates are not transparent, traditional light transmission microscopy is not possible. Several methods were tested to monitor the cells without time-consuming preparation steps. The first method, with the stereomicroscope and fiber optic side illumination (*Fig.4*), showed a monolayer that covered almost the complete surface (*Fig.9*). However, distinguishing individual cells is hard, except at the border were there is more space in between. The second method, with through-the-lens illumination and contrast enhancement with polarizers, on the other hand, did also show the monolayer, but individual cells could still be well distinguished.

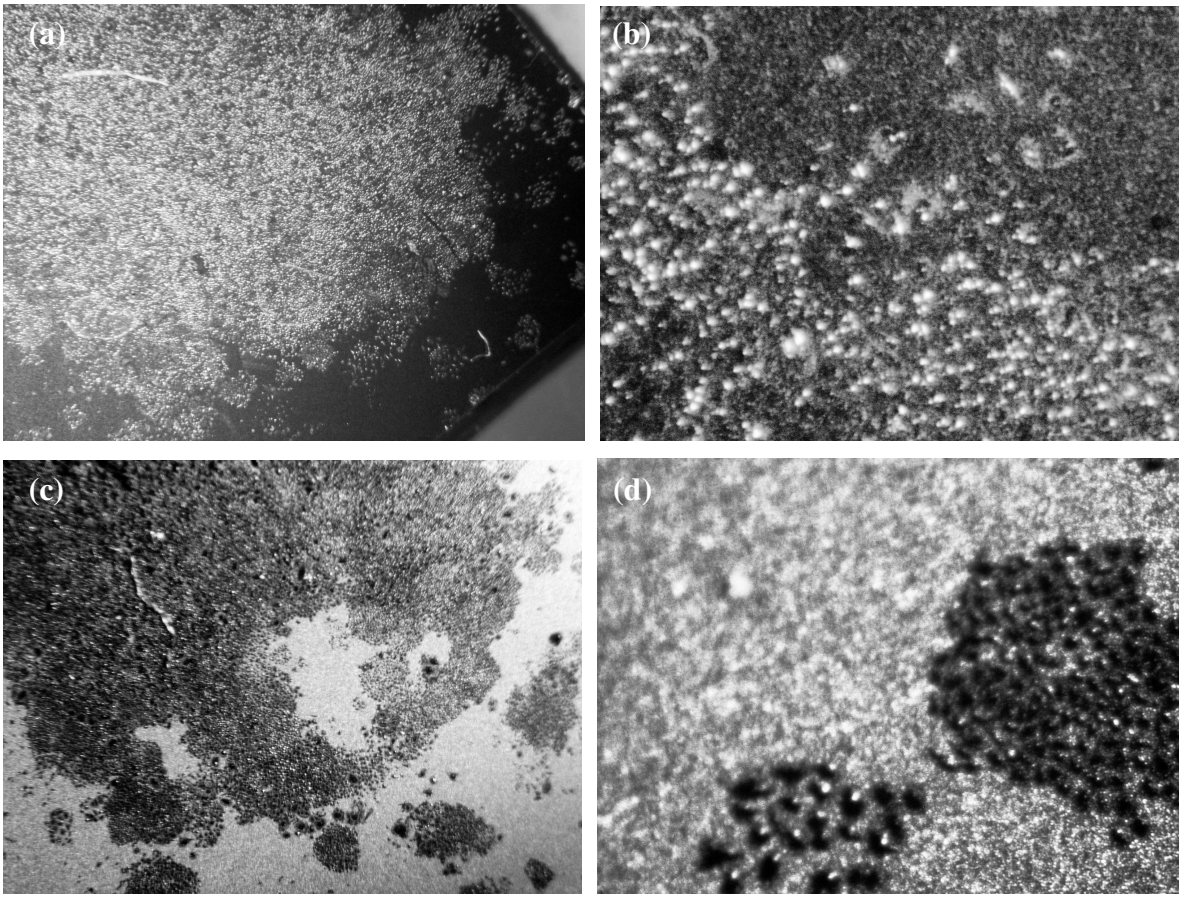

Fig.9: Optical reflection images of CHO cells made with stereomicroscope and side illumination

After 5 days post seeding, cells were fixated as done for SEM imaging. Images were made with a stereomicroscope using side illumination. They were translated from RGB to 8 bit and contrast was enhanced using histogram stretching. (a) and (b) are cells on HT-NCD substrates, (c) and (d) are cells on OT-µCD substrates. Sizes of (a) and (c) are 3.72 mm x 2.75 mm, and sizes of (b) and (d) were 620 µm x 455 µm.

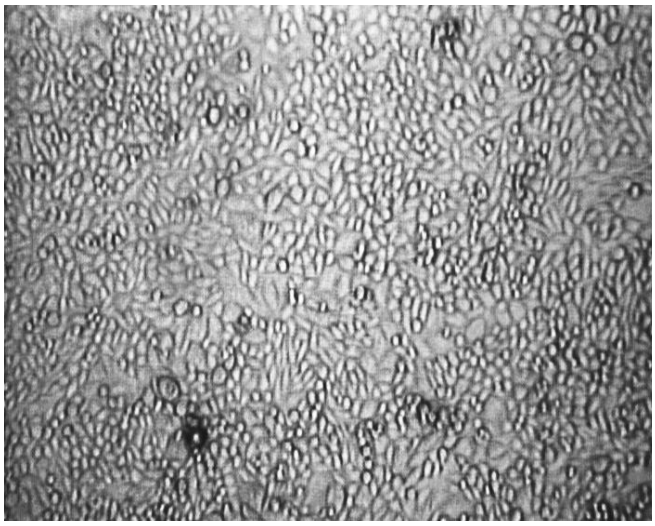

Fig.10: Optical reflection image of a CHO cell monolayer made with a Nikon Optiphot

After 5 days post seeding, cells grown on HT-NCD were fixated as done for SEM imaging. This image was made with a Nikon Optiphot. It was translated from RGB to 8 bit and contrast was enhanced using histogram stretching. Size: 1050 µm x 800 µm

3.2 MTT cell proliferation assay

A better, more quantitative way of assessing cell growth and viability over just visual inspection of cell morphology is the biochemical MTT assay. It was optimized for a number of experimental parameters listed in *Table 2*.

3.2.1 Optimization

Optimization of the MTT cell proliferation assay started with determining the optimal test and reference wavelength. Absorbance spectra of all relevant factors involved were measured (*Fig.11*). The situation at the end of the MTT assay was mimicked by dissolving everything in MTT assay solvent. Even a high concentration of 1 mg/ml MTT did not show any significant absorbance above 500 nm. Cellular reduced MTT-formazan, as well as commercially obtained formazan, had an absorbance maximum at 550 nm. In contrast to earlier published results, there was no difference between these spectra around this wavelength [27]. 6 % (v/v) cell growth medium had a small absorbance between 540 nm and 600 nm. None of the measured absorbance spectra had a significant absorbance above 700 nm. Based on these results, 550 nm was chosen as test wavelength and 800 nm was chosen as reference wavelength.

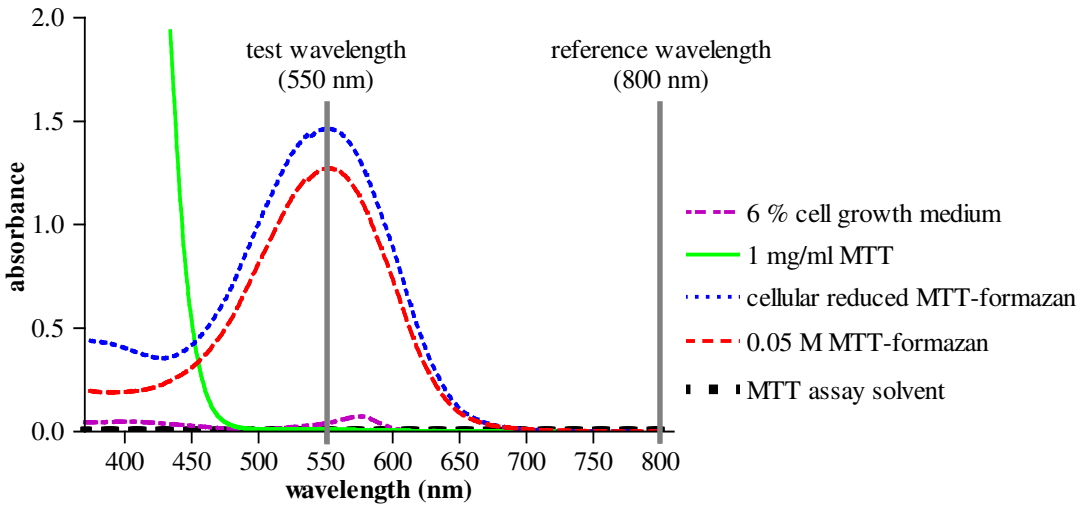

Fig.11: Absorption spectra of MTT, MTT-formazan and cell growth medium

All absorption spectra were obtained in DMSO enriched with 15 % 0.1 M TRIS buffer pH 10 (MTT assay solvent) to mimic the endpoint of the MTT assay. Based on these spectra, 550 nm was chosen as a test wavelength and 800 nm as reference wavelength.

Secondly, the pH-dependence of MTT-formazan absorbance was investigated (*Fig.12a*). In acidified DMSO, the absorbance declines, but the absorbance spectrum is comparable to that obtained in neat DMSO. In contrast, in DMSO with TRIS buffer pH 10 (MTT assay solvent), the absorbance increases together with a marked shift in the spectrum. The absorbance peak shifts from 500 nm to 550 nm. These changes in absorbance spectra are clearly illustrated by the resulting color (*Fig.12b*). This is all very reproducible and consistent with published results [27].

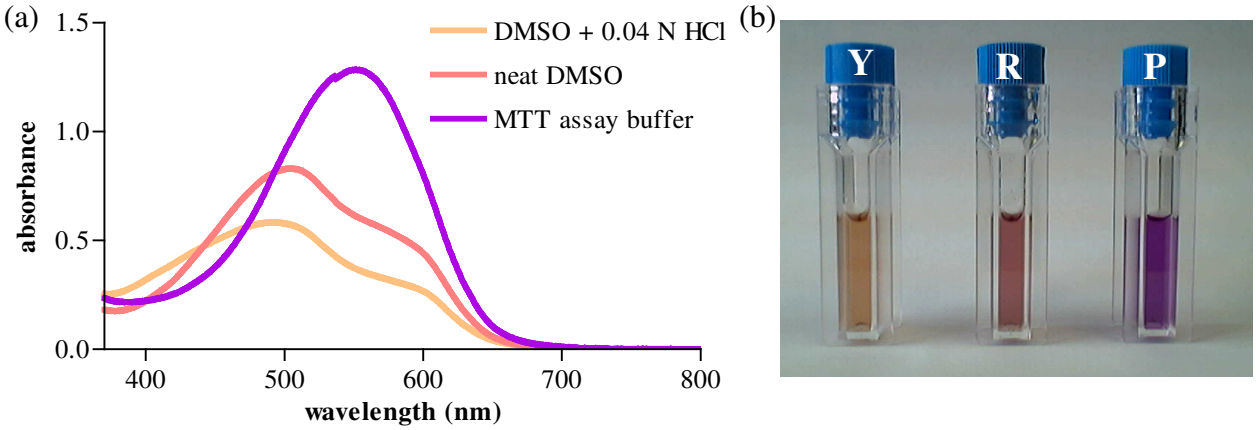

Fig.12: pH-Dependence of formazan absorption spectra

(a) 0.04 M MTT-formazan was dissolved in DMSO acidified with 0.04 N HCl (yellow, Y), in neat DMSO (red, R) and in DMSO with 15 % 0.1 M TRIS buffer pH 10 (MTT assay buffer, purple, P). An obvious shift and increase in the absorbance spectrum of MTT-formazan can be seen with increasing pH-value (a). This shift is reflected in a color difference between the solutions (b).

Next, the stability of MTT in DMSO with Sorensen's glycine buffer pH 10.5 as well as with TRIS buffer pH 10 was measured (*Fig.13*). In the presence of TRIS buffer, the signal barely varied. In contrast, the instability recorded with Sorensen's glycine buffer is very large. Due to this difference, the TRIS buffer was used in the subsequent MTT experiments.

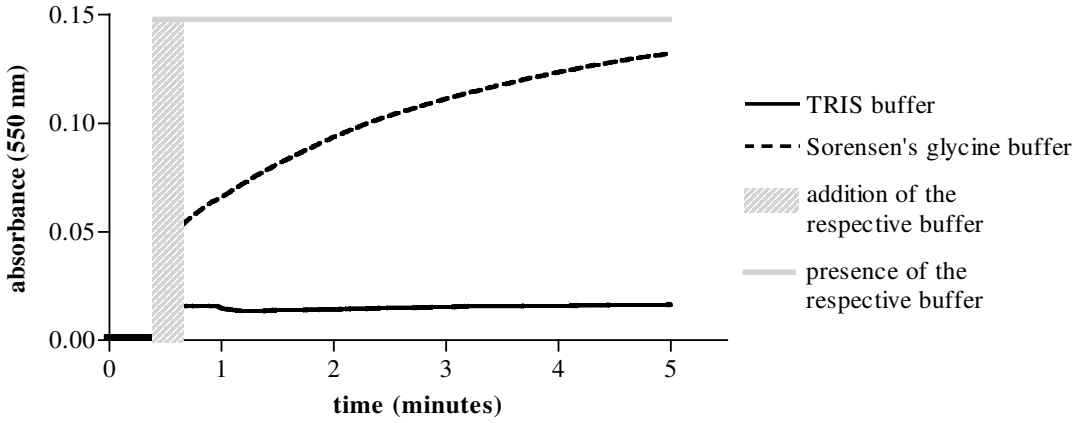

Fig.13: Stability of MTT in DMSO with either TRIS of glycine buffer

As starting solution, 0.5 M MTT was dissolved in neat DMSO. Absorbance was read at 550 nm and after 20 seconds either 0.1 M TRIS buffer pH 10 or 0.1 M Sorensen's glycine buffer pH 10.5 was added to a final concentration of respectively 15 % (v/v) or 11.1 % (v/v). After 5 minutes, the measurement was stopped. The instability of MTT is very much larger for the Sorensen's glycine buffer.

Before application of the TRIS buffer, two factors had to be verified. The first one was the optimal v/v % of buffer in DMSO. To possibly optimize this concentration, a volume dependent curve of MTT-formazan was made (*Fig.14*). Based on this curve, the optimal v/v % would be 3 %. However, this amount is already necessary to buffer only the effect of DMSO. Since reduction of MTT acidifies the solution, the high starting value of 15 % (v/v) was used throughout to certainly buffer the solution. This concentration did not diminish the solubility of the MTT-formazan crystals.

The second factor that had to be verified was the possible interference of cell growth medium. This was investigated by making v/v % dependent curves of cell growth medium in DMSO, both in absence (control) as well as in presence of 15 % (v/v) TRIS buffer pH 10 (*Fig.15a*). This was also compared with results obtained in the presence of 11.1 % (v/v) Sorensen's glycine buffer (pH 10.5) and with published results [27]. In the absence of any buffer, cell growth medium indeed interfered strongly with absorbance measurements. Both buffers used cancelled this effect to a great extent. However, at higher concentrations, TRIS buffer cancelled this interference better than did the Sorensen's glycine buffer. Compared with results obtained by Plumb et al., our methodology gave a larger error for both buffers used.

This is surprising since the composition of our Sorensen's glycine buffer is identical to the published one.

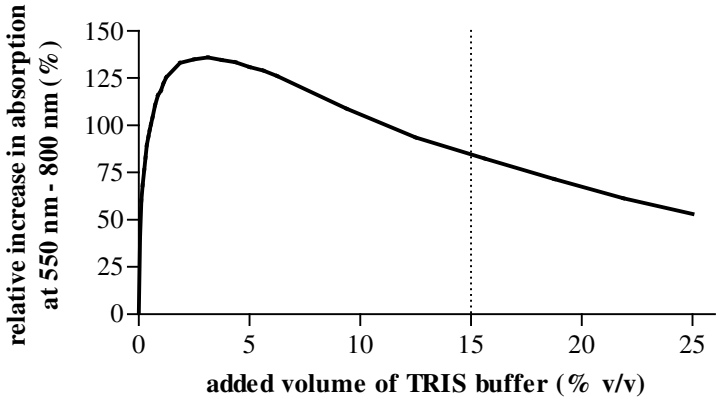

Fig.14: Determination of the optimal concentration of TRIS buffer

To determine the optimal v/v % of TRIS buffer in DMSO, 0.04 M MTT-formazan dissolved in neat DMSO was used as starting solution to which several volumes of 0.1 M TRIS buffer pH 10 was added, expressed in percentage of final volume. Absorbance was measured with 550 nm as test wavelength and 800 nm as reference wavelength. A maximum in absorbance can be seen at 3 %, but 15 % was finally chosen as the optimal concentration TRIS buffer.

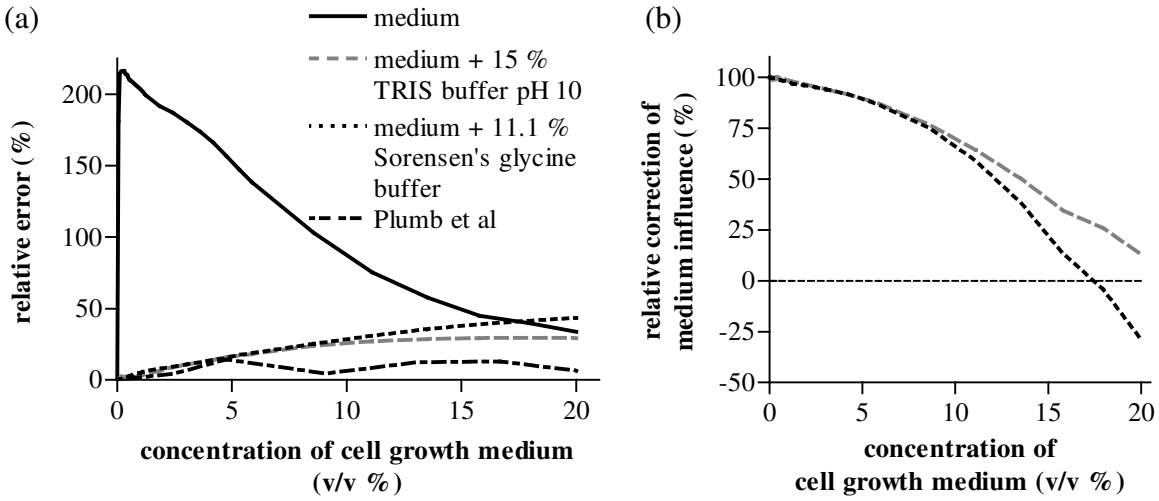

Fig.15: Influence of residual cell growth medium

In (a), the relative error induced by cell growth medium left behind after aspiration, is shown. A solution of 0.04 M MTT-formazan in DMSO, in DMSO with 15 % 0.1 M TRIS buffer pH 10 and in DMSO with 11.1 % 0.1 M Sorensen's glycine buffer pH 10.5 was used as starting solution to which several volumes of cell growth medium were added, expressed in percentage of starting volume. Also the result obtained by Plumb at al. [27] is shown in the same way. This clearly indicates that the effect of the cell growth medium is largely dampened by the presence of a buffer. In (b) The relative correction of the induced error is shown. 100 % meaning complete correction (ideal situation), 0 % meaning no correction at all and negative % meaning an even worse effect. Up to 10 % added cell growth medium, both buffers have the same effect, with TRIS buffer having a better effect above this value.

To better compare the two buffers used, a different presentation of the results was made (*Fig.15b*). In this figure, it is clear that both buffers have the same effect when the concentration of the cell growth medium is less than 10 % (v/v). The estimated residual volume of cell growth medium after aspiration is calculated to be 10 µl, which would lead to a concentration of 1.24 % (v/v) in the added volume of MTT assay solvent. Consequently, The error caused by the cell growth medium is reduced from 200 % to less then 2 % as can be seen in *Fig.15a*.

After optimizing the factors involved with the absorbance readings at the end of the assay, cell specific parameters were optimized. The first parameter was the final MTT concentration in the incubation medium (*Fig.16*). The relationship between final MTT concentration in the incubation medium and absorbance, i.e. MTT reduction, is linear for MTT concentrations up to 1.25 mg/ml, after what it declines. Based on this result, 1.0 mg/ml was chosen as the optimal final MTT concentration in the incubation medium.

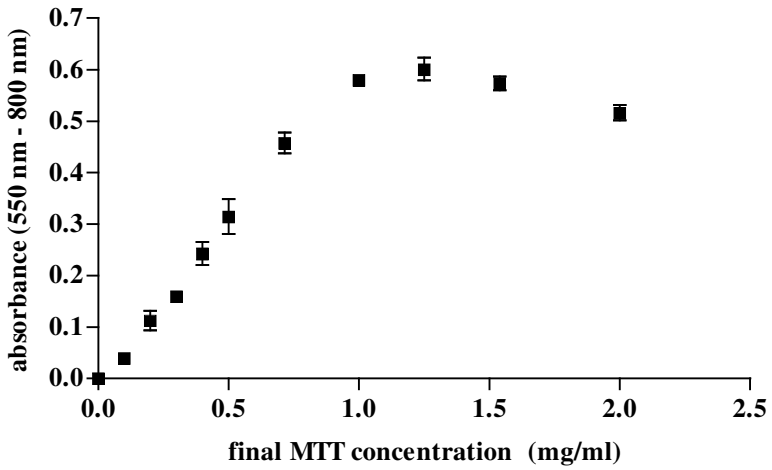

Fig.16: Optimization of the final MTT concentration in the incubation medium

To find the optimal final MTT concentration, 150,000 CHO cells were incubated for 1 hour with various concentrations of MTT. After this incubation period, the solution was aspirated and MTT-formazan crystals were dissolved with MTT assay solvent. The absorbance was measured at 550 nm test wavelength and 800 nm reference wavelength. A clear concentration dependent MTT reduction is demonstrated and the optimal final MTT concentration is determined to be 1.0 mg / ml.

The second optimized cell-dependent parameter was the incubation time. This was done by incubation of a serial dilution of cell densities during either 1 or 4 hours. This resulted in two cell number – MTT-formazan absorbance relationships (*Fig.17a*). After 1 hour, this relationship is linear to about 400,000 cells, while after 4 hours, this relationship is linear up

to 1,500,000 cells. However, due to the estimated number of cells present on the substrates, 1 hour incubation was found to be enough. To control whether this relationship goes through the origin, a linear regression was performed on the data points of 1 hour up to 400,000 cells (*Fig.17b*). The resulting equation (y = 0.06165x + 0.05509) had a good fit (R^2 = 0.9848) and when the X-value, i.e. cell number, would be 0, the confidence interval of the corresponding Y-value was [-0.02981 to 0.1400].

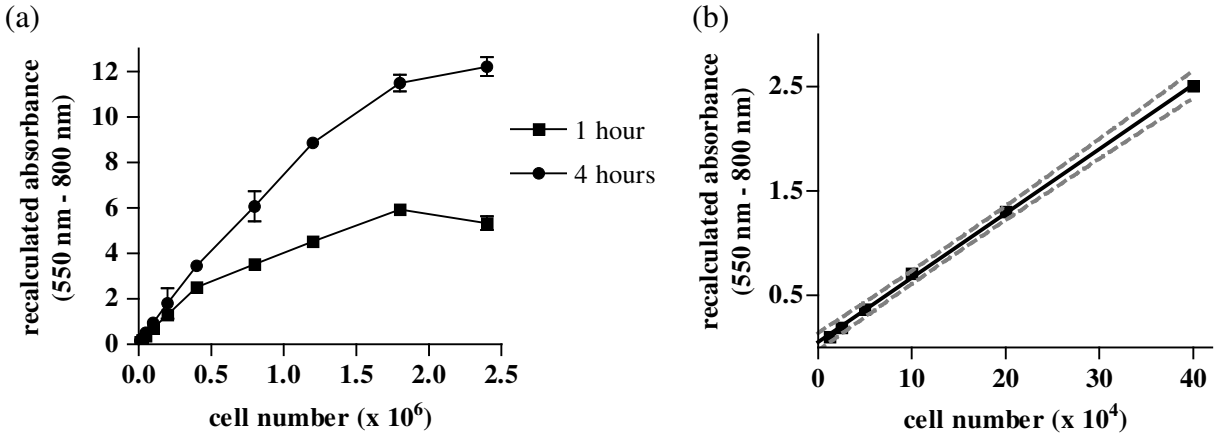

Fig.17: Effect of incubation time on cell number - MTT-formazan absorbance relationship

(a) Relationship between cell number and MTT-formazan absorbance. Absorbances were measured at 550 nm test wavelength and 800 nm reference wavelength. After 1 hour incubation, a linear relationship can be seen for a cell density of 400,000 cells, while after 4 hours, the absorbance was linear to about 1,500,000 cells. (b) expanded lower left region of figure (a). Data points up to 400,000 cells after 1 hour incubation show a linear relationship, expressed by the equation y = 0.06165x + 0.05509. R^2 = 0.9848. Gray lines are the 95% confidence interval.

Prior to application of the now optimized MTT assay, two more parameters concerning the study design needed to be controlled. One of them was the influence of the seeding of the cells, as stated by Wan et al. [25]. An experiment with glass substrates of the same size was executed in order to keep all parameters as much as possible the same. The resulting variance was small and no significant difference between the randomized nor the non-randomized groups could be demonstrated *(Fig.18a*). As a result, the seeding of the cells had an ignorable small influence. Nevertheless, a randomized design was used. Secondly, the method to normalize all substrates to 1 cm^2 was investigated. Glass substrates of different sizes were used, but no significant difference could be demonstrated (*Fig.18b*).

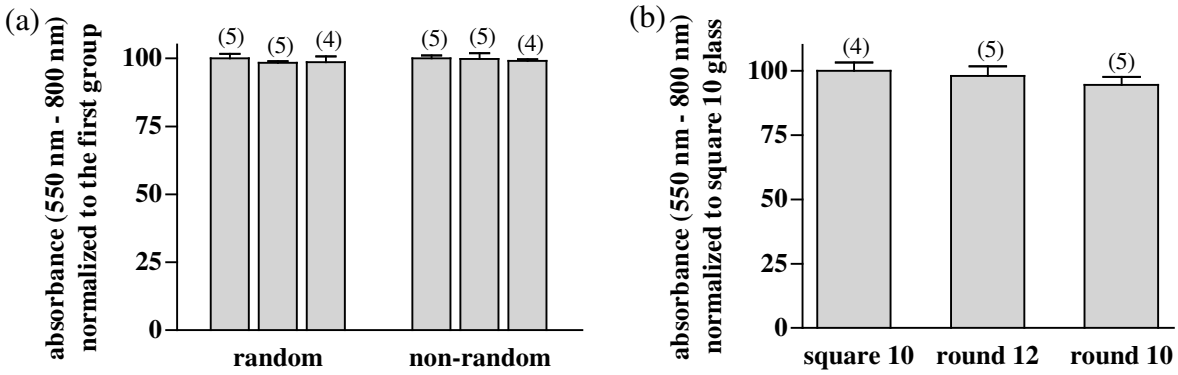

Fig.18: Effect of the study design

(a) Cells were seeded onto glass substrates of equal size and all parameters were kept as much as possible the same. Both the randomized as the non-randomized group were not significantly different. (b) Cells were seeded onto glass of different sizes: square glass substrates of 10 by 10 mm (square 10) and round glass substrates of 12 (round 12) and 10 (round 10) mm in diameter. No statistically significant difference could be demonstrated with one-way ANOVA (numbers in parenthesis indicate the number of samples n).

Since the nanocrystalline wafers were heterogeneous in color due to optical interference effects, the effect of this color on cell growth and viability was investigate using the MTT assay (*Fig.19*). Yellow and blue colored HT-NCD samples were used. After 5 days post seeding, no significant difference was found using an unpaired t-test. Furthermore, there was also no difference between the control glass substrates and the tested HT-NCD substrates (one-way ANOVA analysis). As a result, the nanocrystalline samples were randomly used, regardless of their color.

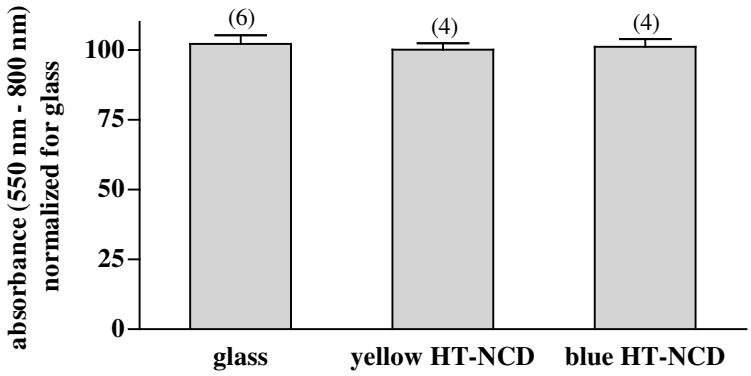

Fig.19: Effect of NCD film layer color

The effect of the NCD color was investigated using yellow and blue HT-NCD substrates. No significant difference between these those two groups nor in comparison with control glass substrates could be demonstrated.

3.2.2 Application of the MTT cell proliferation assay

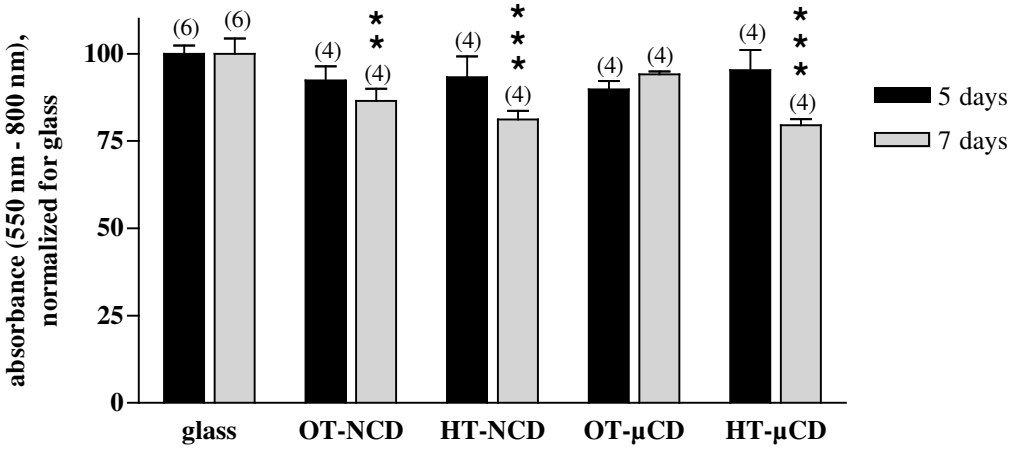

Fig.20: Comparison of NCD and µCD with control glass substrates using the MTT assay

NCD and µCD, either OT or HT, were compared with glass substrates using the MTT assay. Absorbance was normalized to both 1 cm^2 and to control glass substrates. 5 days post seeding (black), no significant difference was demonstrated. Conversely, 7 days post seeding (gray) a significant difference was present ($p<0.01$). Significance levels shown are from comparison with control glass substrates. (** = $p<0.01$, *** = $p<0.001$)

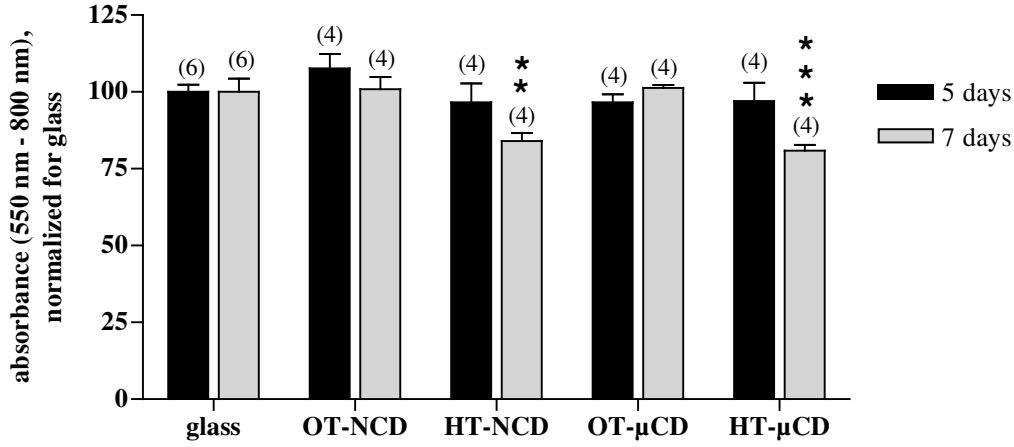

Fig.21: MTT assay corrected for total protein content

The results from *Fig.20* were divided by the total protein content, i.e. results obtained with the Bradford assay. Results after 5 days post seeding (black) were still not significant. Conversely, after 7 days post seeding (gray) a significant difference was still present ($p<0.01$). Significance levels shown are from comparisons with control glass substrates. (** = $p<0.01$, *** = $p<0.001$)

Finally, the optimized MTT assay was applied to investigate possible differences between glass control substrates and NCD and µCD substrates, either oxygen or hydrogen terminated. Two comparable experiments were executed: one took place 5 days post seeding while the second was carried out at 7 days (*Fig.20*). After five days, no significant difference could be demonstrated between the substrates using one-way analysis. In contrast, after 7 days OT and

HT-NCD as well as HT-µCD diamond were significantly different using one-way ANOVA ($p<0.01$). Furthermore, two-way ANOVA did not reveal a significant influence of the type of diamond. On the other hand, surface termination was found to have a significant influence, although only after 7 days ($p<0.01$).

Since the MTT assay measures both cell proliferation and viability, correction for this proliferation leads to data on cell viability solely. Using the data obtained with the Bradford assay, this correction was applied to all MTT data (*Fig.21*). In general, the differences between the control glass substrates and the diamond substrates decreased. After 5 days, still no significant difference could be demonstrated using one-way ANOVA. On the other hand, the differences after 7 days were still significant ($p<0.01$), although compared to glass only the HT samples differed significantly. Conversely, two-way ANOVA revealed an even more significant effect of surface termination after 7 days ($p<0.0001$).

3.3 Bradford assay

A straigthforward endpoint of cell proliferation is the total cell number. Determining the total protein content is a good estimate of this number. The Bradford assay was applied for this purpose. The R^2-value of the calibration curve with BSA was 0.9998 (*result not shown*). No significant difference could be demonstrated between the control glass substrates and the diamond substrates using one-way ANOVA (*Fig.22*).

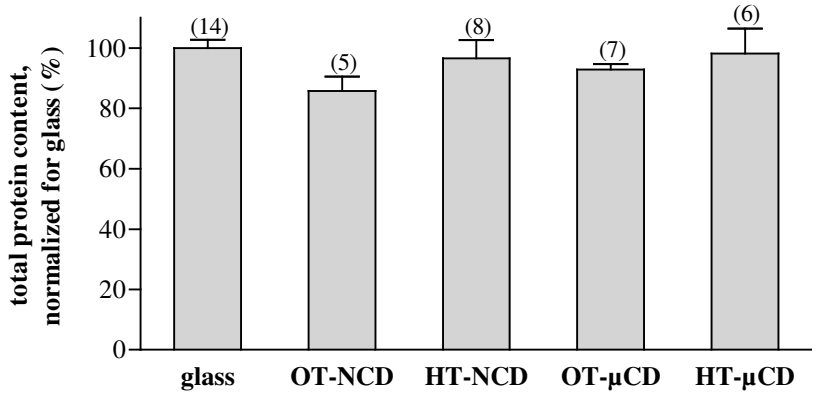

Fig.22: Total protein content of control glass substrates and diamond substrates

6 days post seeding, the total protein content was determined using the Bradford assay. No significant difference between control glass substrates and diamond substrates could be demonstrated.

3.4 [^{3}H]-thymidine cell proliferation assay

To measure the proliferation rate, the [^{3}H]-thymidine cell proliferation assay was used (*Fig.23*). This test was also corrected for total protein content, generating a true proliferation rate. Neither the uncorrected proliferation nor the corrected one are significantly different using one-way ANOVA. This is consistent with the results obtained with the Bradford assay.

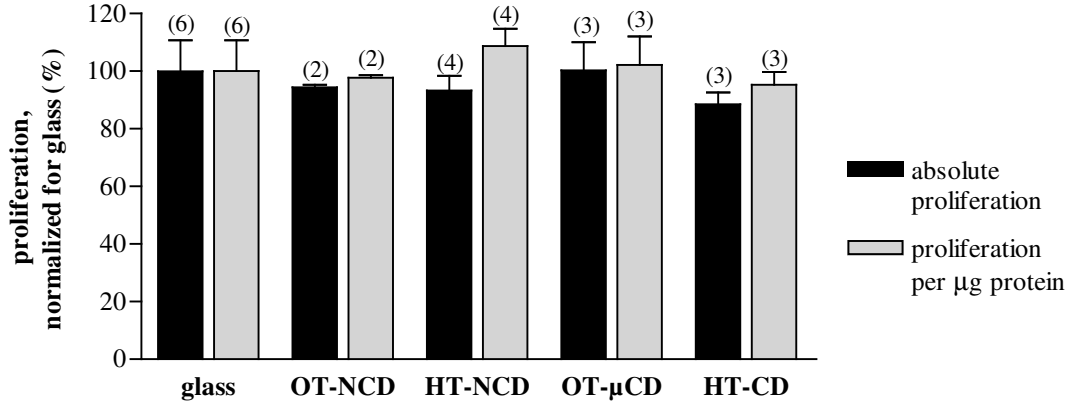

Fig.23: Comparison proliferation of diamond substrates with control glass substrates

[^{3}H]-thymidine cell proliferation assay was used to measure proliferation of cells on control glass substrates and diamond substrates. The uncorrected proliferation (absolute proliferation) as well as the proliferation corrected for the total protein content (proliferation per µg protein) did not show significant differences.

3.5 Flow cytometry

The last applied method to quantify cell viability was flow cytometry. In short, this technique quantifies the cell fractions that are positive for a fluorochrome (*Fig.24*). In this case living cells were indicated by the presence of calcein fluorescence and absence of propidium iodide fluorescence (lower right quadrant in *Fig.24b*). Dead, necrotic cells were characterized by their propidium iodide fluorescence, regardless of calcein fluorescence (upper left and right quadrants in *Fig.24b*). In contrast, dead apoptotic cells were negative for both calcein and propidium iodide fluorescence (lower left quadrant in *Fig.24b*).

Flow cytometry analysis did not show any significant difference between the tested substrate, and this for all cell populations involved (*Fig.25*).

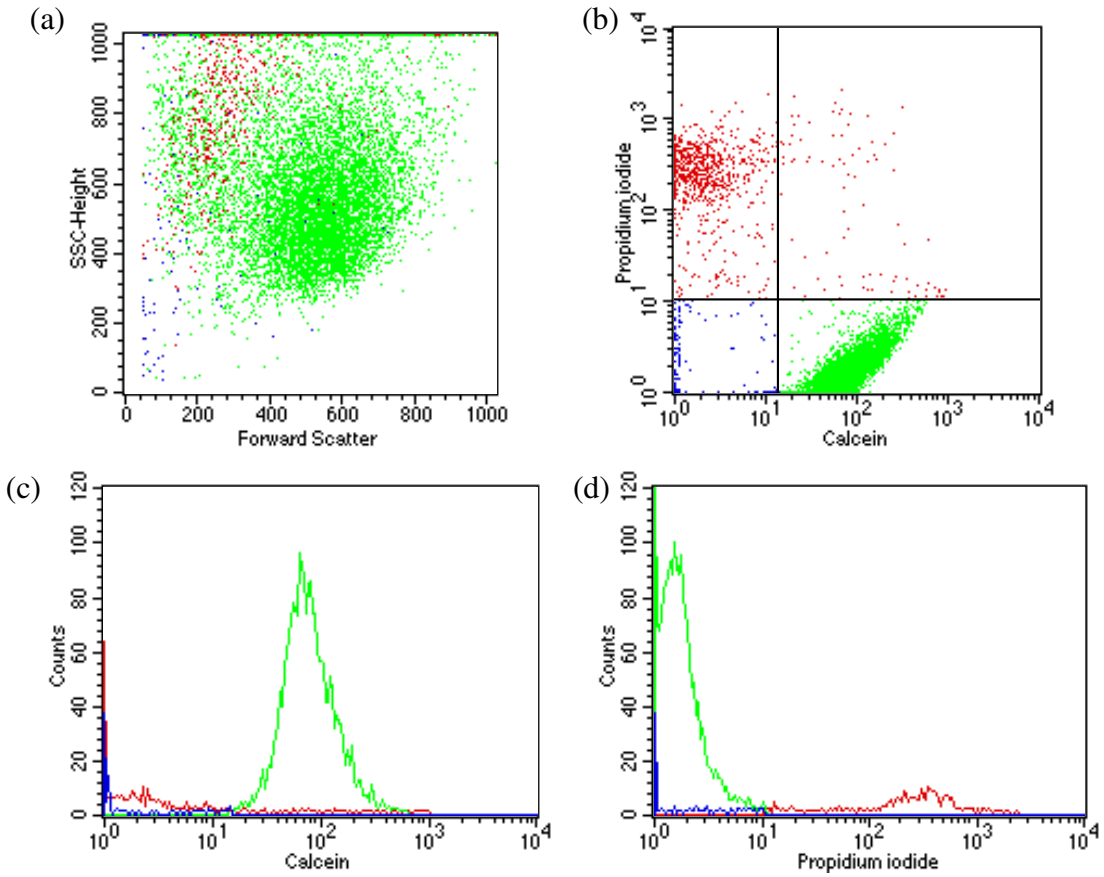

Fig.24: Flow cytometry using calcein-AM and propidium iodide

The result of flow cytometry analysis of one sample is shown. in (a), the scatter plot is shown in which the sideward scatter is plotted against the forward scatter. In (b), the events from the scatter plot are plotted by their fluorescence intensity. This quadrant plot, in which propidium iodide fluorescence is plotted against calcein fluorescence, is used to quantify the fractions of living, necrotic and apoptotic cells. In (c) and (d), the histogram plots of respectively calcein fluorescence and propidium iodide are shown. (green = living cells, red = dead necrotic, blue = dead, apoptotic cells)

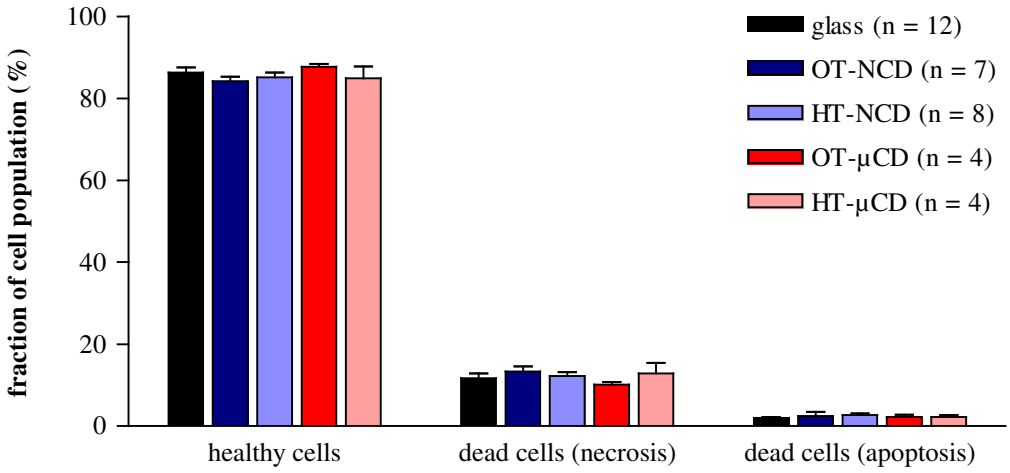

Fig.25: Flow cytometry analysis of healthy, necrotic and apoptotic cells

5 days post seeding, flow cytometry using calcein-AM and propidium iodide was applied to quantify fractions of healthy, necrotic and apoptotic cells. No significant difference could be demonstrated between all substrates tested using one-way ANOVA.

Due to their small size, single crystal diamond substrates were only tested by means of microfluorimetry. This allowed for a combination of visual inspection and a sort of '*in situ*' flow cytometry using calcein-AM and propidium iodide (*Fig.26*). There were no morphological differences between cells on the HT and OT single crystal diamonds and cells on the control glass substrates. It has to be mentioned that the cells on the HT single crystal diamond with surface area of 4 mm^2 were not seeded properly. This was observed by visual inspection of the sample were it was obvious that the starting cell density was too low.

The images obtained were processed with Java based ImageJ and plugins as described in materials and methods. No distinction was made between necrotic and apoptotic cells. Except for the mentioned HT single crystal diamond, the results obtained on diamond are comparable with the ones obtained on glass.

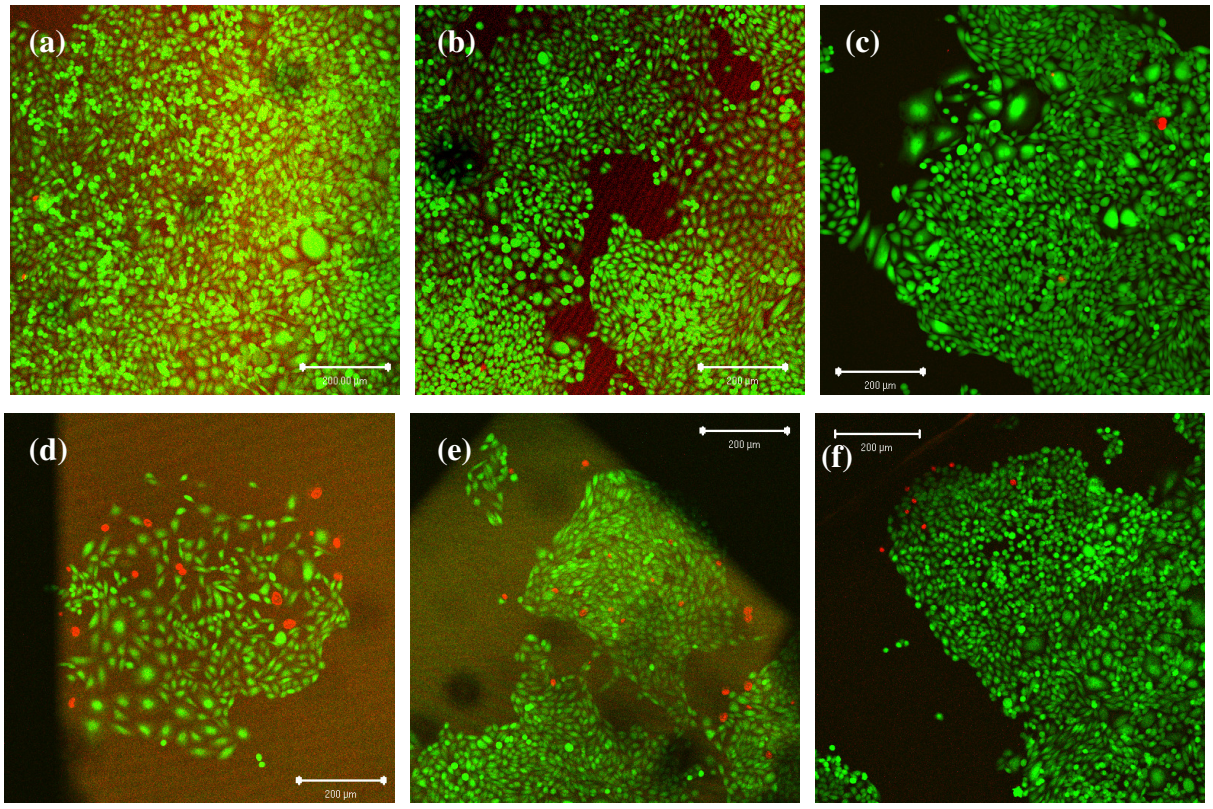

Fig.26: Microfluorimetry using calcein-AM and propidium iodide on single crystal diamond and glass

After 5 days post seeding, CHO cells were incubated with a calcein-AM (green) and propidium iodide (red) loading buffer. Images were taken with a Zeiss LSM 50 META confocal microscope with 10x, NA 0.3 objective. (a) and (b) are cells on respectively HT and OT single crystal diamonds with 6.25 mm^2 surface area. (d) and (e) are cells on respectively HT and OT single crystal diamonds with 4 mm^2 surface area. (c) and (f) are cells on control glass substrates with respectively 6.25 and 4 mm^2 surface area. Scale bars are 200 µm.

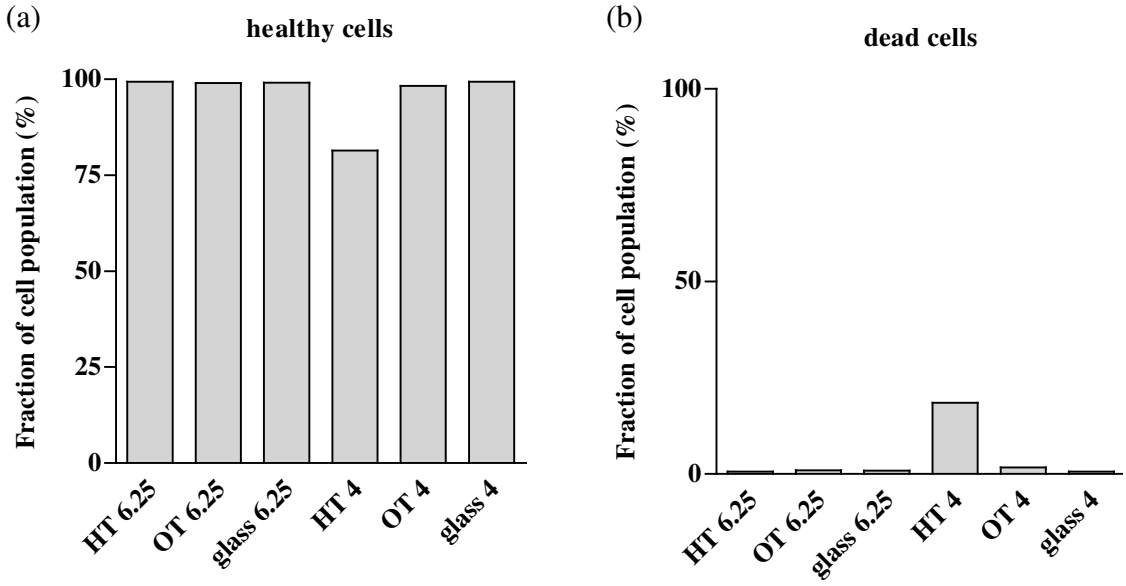

Fig.27: Microfluorimetric analysis of living and dead cells on single crystal diamond

Images obtained for CHO cells on single crystal diamond were processed using Java based ImageJ and plugins. Calcein positive cells were considered as healthy cells (a), while propidium iodide positive cells were considered as dead cells (b). Due to the low sample number (n = 1), no statistics are possible. The high number of dead cells on HT 4 is not representative, since the seeding of cells on this substrate was not successful. (mentioned numbers e.g. HT 6.25, list the surface areas of the square substrates in mm^2)

3.6 Summary of the results

Based on the visual inspection with the scanning electron microscope, neither cell density nor morphology was impeded on any diamond samples, regardless of grain size and surface termination. Although the method with the stereomicroscope and side illumination did not allow distinguishing between individual cells, a normal cell density was also confirmed by the two optical reflection microscopy methods tested. In summary, optical microscopy methods gave consistent results.

This finding was confirmed by the results obtained with biochemical methods. With the exception of the MTT result after 7 days post seeding, all one-way ANOVA analyses indicate a non-significant difference between the means of control glass substrates and the diamond substrates, i.e. HT/OT-NCD and HT/OT-µCD. Furthermore, based on two-way ANOVA analyses of these data neither grain size nor surface termination had a significant influence after 5 days.

4 Discussion and conclusions

Diamond has superior properties compared to conventional semiconductors and is consequently a substrate of great interest for a non-invasive (bio)sensor interface. Together with robust CHO cells stably expressing the embryonic homomeric α_2-glycine receptor, a model interface can be established. This report investigated whether these CHO cells can grow on bare, i.e. uncoated, diamond surfaces and whether they prefer a certain type of diamond and/or surface termination.

Initially it was proposed to grow diamond films on 100 μm thin quartz substrates. This should have allowed simultaneous optical and electronic characterization. After optimization of the growth conditions to prevent the quartz from getting opaque, it appeared during film growth and afterwards while handling that the quartz slivers easily fractured due to mechanical stress imposed by the diamond film and the delicate nature of the material. In order to have ample supply of robust substrates, silicon was finally preferred as substrate.
Also thicker quartz can be used to enable optical characterization with e.g. a 64x , NA 0.9 water objective with a working distance of several mm. However, it takes more time to grow the same amount of samples on this quartz as compared to silicon, since each silicon wafer of 5 cm diameter is equal to about 17 samples of 1 cm^2 while samples on quartz have to be grown one by one.

Since the actual NCD and μCD substrates are non-transparent, other methods than traditional transmission light microscopy had to be applied. Scanning electron microscopy was the first method applied. Although the obtained images are of excellent quality, alteration of cell morphology is possible due to the dehydration step. This step is necessary, yet time consuming, to prevent charging of the cells.
Glass substrates had to be imaged in low vacuum using water vapor to prevent charging effects. The resulting contrast was only moderate compared to the contrast observed on the diamond substrates. Post fixation using osmium tetroxide improved this, probably by enlarging the difference in emitted secondary electrons with respect to glass. Unfortunately, the opposite effect was observed on diamond.
A big advantage of SEM is the possibility to tilt the substrate even to angles of 70 ° with respect to the incoming scanning e-beam. This allows generating a pseudo-3D view of the cells. Besides monolayer areas, aggregates of CHO cells on top of the monolayer could

sometimes be seen. At first, it was thought that the seeding of the cells caused this effect. Yet, even very evenly dispersed cells show this effect after reaching full confluence. The exact cause of this effect is not known, but surface wettability could be responsible in part [23]. Cells may be pushed off the surfaces or just not attach properly, thereby assuming a rounded shape. As a result, they change from adhesive cells towards suspension cells [23].

The other method employed to visualize the cells on the diamond substrates was optical reflection microscopy. The first microscope applied for this method was a stereomicroscope with fiber-optic side-illumination. The resulting images are unfortunately only of moderate quality compared to published images of cells on a non-transparent substrate [7]. There are two likely reasons for this. First, the scale at which the CHO cells have to be visualized is at the limit of the resolution of the microscope applied. Secondly, when the cells are sitting tight in a confluent layer, they screen each other from the side illumination applied and off-edge cells do not stick out enough to be sufficiently reflective. As a result, these images can only be used to describe the dispersion of the cells on the surface.
In contrast, the other microscope, which illuminated the cells through the lens perpendicular to the surface and which also had polarization control, allowed distinguishing individual cells much better. After optimizing optical contrast, the monolayer of cells can properly be visualized, generating images of equal quality compared to published articles [7]. Still, it has to be noted that CHO cells are rather small cells (~20 μm in diameter), while most cell types used for this purpose are rather larger (50 μm in diameter or even more) [5].
Despite all these difficulties encountered, visual inspection of the cells on all substrates did not indicate any disadvantageous influence of the substrates tested.

In addition to visual inspection, biochemical assays were applied to better quantify cell density and viability. All tests carried out before the 7^{th} day post seeding confirm the findings of the visual inspection. However, one remark has to be made.
Results of both the MTT cell proliferation assay and the [^{3}H]-thymidine cell proliferation assay are divided by the results obtained with the Bradford assay. This would generate a measure of respectively cell metabolic activity and cell proliferation rate, at least if the amount of protein per cell is the same for each substrate. This does not necessarily have to be the case [46]. Furthermore, a growth phase-dependent protein expression could occur as seen with bacteria [47]. If we assume that none of these factors occurs, only the variability between experiments can generate erroneous results, since all experiments are executed on different

substrates. To keep this variation as low as possible, as many parameters as possible were equalized for all experiments.

The MTT result after 7 days, which had significant different mean values, indicated the significant negative influence of hydrogen terminated surfaces. Although this is not confirmed by other experiments, it is consistent with the report published by Zhu et al. [23]. Furthermore, a possible explanation of the differences between 5 and 7 days post seeding could be the further advancement in the exponential growth, resulting in larger differences between control and test samples.

Still, based on the acquired results, it is justified to conclude that cell growth and viability on bare nano- and microcrystalline diamond substrates is not substantially attenuated with respect to the glass control, at least not after 6 days. As a consequence, surface termination alone cannot be used to control specific cell positioning. This would require that one of the substrates tested would diminish cell growth and/or viability considerably.
However, if the choice has to be made between bare hydrogen or oxygen terminated support surfaces to grow cells on top of it, preference should be given towards the oxygen terminated surfaces. Furthermore, the type of diamond, NCD or μCD, does not matter. Therefore, other parameters such as ease of film growth, scalability and price of the diamond substrates can be considered.

Since Ariano *et al.* used coated, single crystal diamond, the effect of surface termination is largely cancelled by the coating [20]. However, it has to be noted that surface termination, i.e. wettability, indeed can influence cellular adhesion via alterations in cell adhesion molecule structures[48]. Furthermore, Lee *et al.* have demonstrated that hydrophobic surfaces hamper fibronectin - $\alpha_5\beta_1$ integrin binding, reducing cell adhesion [48].
The effect of grain size, on the other hand, is not straightforward to explain. Unlike most topologies used to study possible effects of topology, diamond surfaces are just ‘rough’. This roughness is thought to aid cell adhesion [49]. Moreover, using Fluorescence Interference Contrast Microscopy (FLIC), the group of Fromherz have shown that a variety of cell types rest on a cushion like extracellular matrix extending from 20 to 100 nm outside the basolateral membrane keeping a distance to the actual semiconductor surface [50]. Similarly, the surface roughness of the diamond surfaces used in this report forms apparently no statistically significant hindrance for the growing and proliferating CHO cells cushioned as they are by

their own ECM. However, if one was able to grow an ensemble of tiny pillars or spikes with irregular height, this could modulate the attractiveness for cell attachment and offer a manner of patterning.

In contrast to results obtained with NCD and μCD, the only results obtained on single crystal diamond was a microfluorimetric analysis of living and dead cells. There are two reasons for this small amount of data. First, their availability is rather limited since they are procured from external commercial suppliers relying on limited, natural diamond sources. Furthermore, the small size of the single crystal diamonds used hampers the seeding of the cells. Surface tension effects of the cell suspension causes the diamonds to be lifted right off the bottom of the well plate by just retracting the pipette tip. As a consequence, they had first to be glued with a very tiny spot of nail polish to a glass coverslip to make them heavier. Moreover, the small surface area requires a very small cell suspension volume. This generates a high variability between the cell densities on the diamond substrates, impeding any quantitative assay.

4.1 MTT assay opimization

Before the MTT cell proliferation was applied, it became clear during the course of the experiments that it had to be optimized first. This optimization procedure requires some explanation. First the parameters affecting absorbance reading are discussed, followed by the cell specific parameters and the study design.

In the original assay, the MTT-formazan crystals are dissolved by addition of acidified isopropanol to the incubation medium [24]. This acidification is necessary to avoid interference of the phenol red present in the cell growth medium with absorbance readings [34]. At the same time, however, protein precipitation occurs due to this acidification. As a consequence, incubation medium deprived of phenol red and/or serum proteins is used [34]. A more straightforward solution, namely aspiration of the incubation medium prior to addition of the solvent, circumvents all these problems and does improve the solubility of the formazan crystals.

Secondly, several solvents have been evaluated for dissolving the MTT-formazan crystals [36-38]. Dimethyl sulfoxide (DMSO) is recognized to be the best solvent, although this solvent is toxic and can have deleterious effects on some plastics. Furthermore, Plumb *et al.* have demonstrated that DMSO alone is not enough [27]. MTT-formazan absorbance

properties also have a strong pH-dependence. Without buffer, high cell densities will be severely underestimated because they reduce many MTT molecules, generating many HBr molecules and thus a low pH. Decreasing the pH leads to a shift of the absorbance spectrum, accompanied with a strong decline of the maximum absorbance value, which was confirmed in the results section. Consequently, a 0.1 M TRIS buffer of pH 10 was used to determine the optimal test and reference wavelength. In contrast to Nikkhah et al. [42], everything was dissolved in DMSO with 15 % (v/v) TRIS buffer to mimic the endpoint of the MTT assay. Because the absorbance peak of MTT-formazan was situated at 550 nm, this wavelength was chosen as test wavelength. Since MTT itself did not significantly absorb at this wavelength, a reference wavelength corrects for instrumentation drift and possible wavelength-dependent optical absorption effects by the cuvette material [34]. Any wavelength above 700 nm can be used for this purpose because none of the tested substances significantly absorbed light in this spectral region. Eventually, 800 nm was chosen as reference wavelength.

After determining the optimal test and reference wavelength, the TRIS buffer with pH 10 was compared with Sorensen's glycine buffer (pH 10.5) used by Plumb *et al.* [27]. MTT was found to be more stable in TRIS buffer than in the glycine buffer. This cannot be explained by the presence of glycine alone, because a 0.1 M glycine solution without adjusted pH did not cause an increased instability of MTT (*results not shown*). Furthermore, absorbance measured in the presence of the Sorensen's glycine buffer was about 0.3 times higher than that measured in the presence of the TRIS buffer (*results not shown*). Based on these results, the TRIS buffer was chosen.

The last factor involved in absorbance readings was the influence of the cell growth medium. The *absorbanc*e of this medium itself was insignificant. Nevertheless, the cell growth medium itself had a large influence. Clearly a pH effect was observed, because addition of a buffer cancelled this effect almost completely at low volumes of cell growth medium.

After optimizing the cell specific parameters, i.e. final MTT concentration and incubation time, the study design of the MTT assay was investigated. Since neither the seeding of the cell onto the substrates nor the normalization procedure influences the final result, the optimized MTT assay is a reliable assay.

5 Future directions

Since neither the type of diamond nor its surface termination can be used to control cell positioning, other means of cell patterning have to be investigated and/or developed. Because CHO cells have little or no preference for some types of surfaces, cell resistant regions must be created. This could be done either by chemical modification of the surface or by changing the topology of the diamond or both.

Secondly, further steps towards a non-invasive interface must be undertaken, meaning that FET structures should be tested while controlling the membrane potential of the cell with a patch clamp pipette.

List of references

1. Albrecht DR, Underhill GH, Wassermann TB, Sah RL, Bhatia SN. Probing the role of multicellular organization in three-dimensional microenvironments. Nat Methods 2006; 3(5):369-75.

2. Kusterer J, Alekov A, Pasquarelli A *et al*. A diamond-on-silicon patch-clamp-system. Diamond Relat Mater 2005; 14:2139-42.

3. Gray DS, Tan JL, Voldman J, Chen CS. Dielectrophoretic registration of living cells to a microelectrode array. Biosens Bioelectron 2004; 19:1765-74.

4. Kane RS, Takayama S, Emanuele O, Ingber DE, Whitesides GM. Patterning proteins and cells using soft lithography. Biomaterials 1999; 20:2363-76.

5. Fromherz P, Offenhäusser A, Vetter T, Weis J. A neuron-silicon junction: a Retzius cell of the leech on an insulated-gate field-effect transistor. Science 1991; 252(5010):1290-3.

6. Brittinger M, Fromherz P. Field-effect transistor with recombinant potassium channels: fast and slow response by electrical and chemical interactions. Appl Phys A 2005; 81:439-47.

7. Bogner E, Dominizi K, Hagl P *et al*. Bridging the gap - Biocompatibility of microelectronic materials. Acta Biomaterialia 2006; 2:229-37.

8. Sugata K, Tachiki M, Fukuda T, Seo H, Kawarada H. Nanoscale modification of the hydrogen terminated diamond surface using atomic force microscope. Jpn J Appl Phys 2002; 41:4983-6.

9. Nichols BM, Butler JE, Russell J.N. , Hamers RJ. Photochemical functionalization of hydrogen-terminated diamond surfaces: a structural and mechanistic study. J Phys Chem B 2005; 109(44):2020938-20947.

10. Hartl A, Schmich E, Garrido JA *et al*. Protein-modified nanocrystalline diamond thin films for biosensor applications. Nat Mater 2004; 3(10):736-42.

11. Yang W, Auciello O, Butler JE *et al*. DNA-modified nanocrystalline diamond thin-films as stable, biologically active substrates. Nat Mater 2002; 1(4):253-7.

12. Christiaens P, Vermeeren V, Wenmackers S *et al*. EDC-mediated DNA attachment to nanocrystalline CVD diamond films. Biosens Bioelectron 2006; *article in press*.

13. Lasseter TL, Clare BH, Abbott NL, Hamers RJ. Covalently modified silicon and diamond surfaces: resistance to nonspecific protein adsorption and optimization for biosensing. J Am Chem Soc 2004; 126(33):10220-1.

14. Garrido JA, Nebel CE, Todt R *et al*. Novel in-plane gate devices on hydrogenated diamond surfaces. Phys Stat Sol (a) 2003; 199(1):56-63.

15. Nordsletten L, Hogasen AK, Konttinen YT, Santavirta S, Aspenberg P, Aasen AO. Human monocytes stimulation by particles of hydroxyapatite, silicon carbide and diamond: in vitro studies of new prosthesis coatings. Biomaterials 1996; 17(15):1521-7.

16. Tang L, Tsai C, Gerberich WW, Kruckeberg L, Kania DR. Biocompatibility of chemical-vapour-deposited diamond. Biomaterials 1995; 16(6):483-8.

17. Garguilo JM, Davis BA, Buddie M, Köck FAM, Nemanich RJ. Fibrinogen adsorption onto microwave plasma chemical vapor deposited diamond films. Diamond Relat Mater 2004; 13(4-8):595-9.

18. Cui FZ, Li DJ. A review of investigations on biocompatibility of diamond-like carbon and carbon nitride films. Surf Coatings Technol 2000; 131:481-7.

19. Specht CG, Williams OA, Jackman RB, Schoepfer R. Ordered growth of neurons on diamond. Biomaterials 2004; 25(18):4073-8.

20. Ariano P, Baldelli P, Carbone E *et al*. Cellular adhesion and neuronal excitability on functionalised diamond surfaces. Diamond Relat Mater 2005; 14:669-74.

21. Mangin JM, Baloul M, Prado De Carvalho L, Rogister B, Rigo JM, Legendre P. Kinetic properties of the alpha2 homo-oligomeric glycine receptor impairs a proper synaptic functioning. J Physiol 2003; 553(Pt 2):369-86.

22. Schmidtner M, Fromherz P. Functional Na+ Channels in Cell Adhesion probed by Transistor Recording. Biophys J 2006; 90(1):183-9.

23. Zhu B, Lu Q, Yin J , Hu J, Wang Z. Effects of laser-modified polystyrene substrate on CHO cell growth and alignment. J Biomed Mater Res B 2004; 70B:43-8.

24. Mosmann T. Rapid colorimetric assay for cellular growth and survival: application to proliferation and cytotoxicity assays. J Immunol Methods 1983; 65:55-63.

25. Wan H, Williams R, Doherty P, Williams DF. A study of the reproducibility of the MTT test. J Mater Sci Mater Med 1994; 5:154-9.

26. Okpalugo TI, McKenna E, Magee AC, McLaughlin J, Brown NM. The MTT assays of bovine retinal pericytes and human microvascular endothelial cells on DLC and Si-DLC-coated TCPS. J Biomed Mater Res A 2004; 71(2):201-8.

27. Plumb JA, Milroy R, Kaye SB. Effects of the pH dependence of 3-(4,5-dimethylthiazol-2-yl)-2,5-diphenyl-tetrazolium bromide-formazan absorption on chemosensitivity determined by a novel tetrazolium-based assay. Cancer Res 1989; 49(16):4435-40.

28. Berridge MV, Herst PM, Tan AS. Tetrazolium dyes as tools in cell biology: New insights into their cellular reduction. Biotechnol Annu Rev 2005; 11:127-52.

29. Berridge MV, Tan AS. Characterization of the cellular reduction of 3-(4,5-dimethylthiazol-2-yl)-2,5-diphenyltetrazolium bromide (MTT): subcellular localization, substrate dependence, and involvement of mitochondrial electron transport in MTT reduction. Arch Biochem Biophys 1993; 303(2):474-82.

30. Liu Y, Peterson DA, Kimura H, Schubert D. Mechanism of cellular 3-(4,5-dimethylthiazol-2-yl)-2,5-diphenyltetrazolium bromide (MTT) reduction. J Neurochem 1997; 69(2):581-93.

31. Marshall NJ, Goodwin CJ, Holt SJ. A critical assessment of the use of microculture tetrazolium assays to measure cell growth and function. Growth Regul 1995; 5(2):69-84.

32. Park JG, Kramer BS, Steinberg SM *et al*. Chemosensitivity testing of human colorectal carcinoma cell lines using a tetrazolium-based colorimetric assay. Cancer Res 1987; 47(22):5875-9.

33. Slater TF, Sawyer B, Straeuli U. Studies on succinate-tetrazolium reductase systems. III. Points of coupling of four different tetrazolium salts. Biochim Biophys Acta 1963; 77:383-93.

34. Denizot F, Lang R. Rapid colorimetric assay for cell growth and survival. Modifications to the tetrazolium dye procedure giving improved sensitivity and reliability. J Immunol Methods 1986; 89(2):271-7.

35. Vistica DT, Skehan P, Scudiero D, Monks A, Pittman A, Boyd MR. Tetrazolium-based assays for cellular viability: a critical examination of selected parameters affecting formazan production. Cancer Res 1991; 51(10):2515-20.

36. Alley MC, Scudiero DA, Monks A *et al*. Feasibility of drug screening with panels of human tumor cell lines using a microculture tetrazolium assay. Cancer Res 1988; 48(3):589-601.

37. Twentyman PR, Luscombe M. A study of some variables in a tetrazolium dye (MTT) based assay for cell growth and chemosensitivity. Br J Cancer 1987; 56(3):279-85.

38. Carmichael J, DeGraff WG, Gazdar AF, Minna JD, Mitchell JB. Evaluation of a tetrazolium-based semiautomated colorimetric assay: assessment of chemosensitivity testing. Cancer Res 1987; 47(4):936-42.

39. Jabbar SA, Twentyman PR, Watson JV. The MTT assay underestimates the growth inhibitory effects of interferons. Br J Cancer 1989; 60(4):523-8.

40. Heo DS, Park JG, Hata K, Day R, Herberman RB, Whiteside TL. Evaluation of tetrazolium-based semiautomatic colorimetric assay for measurement of human antitumor cytotoxicity. Cancer Res 1990; 50(12):3681-90.

41. Scudiero DA, Shoemaker RH, Paull KD *et al*. Evaluation of a soluble tetrazolium/formazan assay for cell growth and drug sensitivity in culture using human and other tumor cell lines. Cancer Res 1988; 48(17):4827-33.

42. Nikkhah G, Tonn JC, Hoffmann O *et al*. The MTT assay for chemosensitivity testing of human tumors of the central nervous system. Part I: Evaluation of test-specific variables. J Neurooncol 1992; 13(1):1-11.

43. Goodwin CJ, Holt SJ, Downes S, Marshall NJ. The use of intermediate electron acceptors to enhance MTT bioreduction in a microculture tetrazolium assay for human growth hormone. Life Sci 1996; 59(20):1745-53.

44. Kampmeier J, Baldysiak-Figiel A, de Jong-Hesse Y, Lang GK, Lang GE. Effect of growth factors on proliferation and expression of growth factor receptors in a human lens epithelial cell line. J Cataract Refract Surg 2006; 32(3):510-4.

45. Berry SD, Weber Nielsen MS, Sejrsen K, Pearson RE, Boyle PL, Akers RM. Use of an immortalized bovine mammary epithelial cell line (MAC-T) to measure the mitogenic activity of extracts from heifer mammary tissue: effects of nutrition and ovariectomy. Domest Anim Endocrinol 2003; 25(3):245-53.

46. Hasinoff BB, Abram ME, Chee GL *et al*. The catalytic DNA topoisomerase II inhibitor dexrazoxane (ICRF-187) induces endopolyploidy in Chinese hamster ovary cells. J Pharmacol Exp Ther 2000; 295(2):474-83.

47. Walker SL, Hill JE, Redman JA, Elimelech M. Influence of growth phase on adhesion kinetics of Escherichia coli D21g. Appl Environ Microbiol 2005; 71(6):3093-9.

48. Lee MH, Ducheyne P, Lynch L, Boettiger D, Composto RJ. Effect of biomaterial surface properties on fibronectin-alpha5beta1 integrin interaction and cellular attachment. Biomaterials 2006; 27(9):1907-16.

49. Curtis A, Wilkinson C. Topographical control of cells. Biomaterials 1997; 18(24):1573-83.

50. Braun D, Fromherz P. Fluorescence interferometry of neuronal cell adhesion on micro structured silicon. Phys Rev Lett 1998; 81:5241-4.

Auteursrechterlijke overeenkomst

Opdat de Universiteit Hasselt uw eindverhandeling wereldwijd kan reproduceren, vertalen en distribueren is uw akkoord voor deze overeenkomst noodzakelijk. Gelieve de tijd te nemen om deze overeenkomst door te nemen en uw akkoord te verlenen.

Ik/wij verlenen het wereldwijde auteursrecht voor de ingediende eindverhandeling:
Cell viability on functionalized diamond surfaces: towards non-invasive monitoring of cell characteristics
Richting: **Master in de biomedische wetenschappen** Jaar: **2006**
in alle mogelijke mediaformaten, - bestaande en in de toekomst te ontwikkelen - , aan de Universiteit Hasselt.

Deze toekenning van het auteursrecht aan de Universiteit Hasselt houdt in dat ik/wij als auteur de eindverhandeling, - in zijn geheel of gedeeltelijk -, vrij kan reproduceren, (her)publiceren of distribueren zonder de toelating te moeten verkrijgen van de Universiteit Hasselt.

U bevestigt dat de eindverhandeling uw origineel werk is, en dat u het recht heeft om de rechten te verlenen die in deze overeenkomst worden beschreven. U verklaart tevens dat de eindverhandeling, naar uw weten, het auteursrecht van anderen niet overtreedt.

U verklaart tevens dat u voor het materiaal in de eindverhandeling dat beschermd wordt door het auteursrecht, de nodige toelatingen hebt verkregen zodat u deze ook aan de Universiteit Hasselt kan overdragen en dat dit duidelijk in de tekst en inhoud van de eindverhandeling werd genotificeerd.

Universiteit Hasselt zal u als auteur(s) van de eindverhandeling identificeren en zal geen wijzigingen aanbrengen aan de eindverhandeling, uitgezonderd deze toegelaten door deze licentie

Ik ga akkoord,

Nick SMISDOM

Datum: